ABSTRACT

Title of Thesis: WATER MIST SUPPRESSION IN A
TURBULENT LINE BURNER

Elizabeth Cyler Keller, Master of Science, 2016

Thesis Directed By: Associate Professor André W. Marshall, Ph.D.,
Department of Fire Protection Engineering

An experimental study of water mist fire suppression in a buoyant, turbulent diffusion flame is presented. An existing turbulent line burner facility was modified to allow for water mist suppression. These modifications include streamlining the oxidizer delivery system, facility improvements to increase mist generation efficiency, as well as the addition of a mist containment system and an enhanced exhaust flow to homogenize the water mist in the flame region and reduce secondary flows. Following these improvements, the capabilities of the water mist generation system were characterized both using a classical mass balance approach and using more modern advanced diagnostic techniques. The turbulent line burner facility fitted with the water mist improvements were applied to suppress a 50 kW methane flame. Species-based calorimetry was used to evaluate the global heat release rate and combustion efficiency to evaluate suppression behavior. Detailed local measurements of flame temperature were also performed and provide a useful data set for the evaluation of flame suppression response and for the validation of CFD fire models.

WATER MIST SUPPRESSION IN A TURBULENT LINE BURNER

by

Elizabeth Cyler Keller

Thesis submitted to the Faculty of the Graduate School of the
University of Maryland, College Park, in partial fulfillment
of the requirements for the degree of
Master of Science
2016

Advisory Committee:
 Professor André Marshall, Chair
 Professor Arnaud Trouvé
 Professor Michael Gollner

Dedication

For Mom, who never stopped believing that I could accomplish more when settling seemed like the thing to do.

Acknowledgements

Additional thanks go to my colleagues in the field, both past and present, who provided me the initial challenge and strength of will to succeed far beyond what I originally set out to do.

Final thanks go to my family: to my mother Wanda, father Laney, sister Suzanne, grandmother Hazel, grandfather Fred, and niece Samantha Allison for their unending support and encouragement through all of the highs and lows. You never gave up on me and allowed me to believe that I could finally finish what was started.

Table of Contents

List of Tables

List of Figures

Nomenclature

Acronyms and Abbreviations

CDG	carbon dioxide generation
CFD	computational fluid dynamics
CH_4	methane
cm	centimeter
CO	carbon monoxide
CO_2	carbon dioxide
d	representative diameter
DAQ	data acquisition
g	gram
H_2O	water
Hz	hertz
J	Joule
K	Kelvin
kW	kilowatt
m	meter
MEC	minimum extinguishing concentration
mm	millimeter
N_2	Nitrogen
NFPA	National Fire Protection Association
nm	nanometer
O_2	oxygen
OC	oxygen consumption
RH	relative humidity
TLB	turbulent line burner
VF	volume fraction
s	second
μm	micron

Equation Variables

A_{ox}	cross sectional area
α	absorbance
b	particle field distance
C_f^{ox}	flow coefficient characterizing the velocity distribution
c_p	heat capacity at constant pressure
C_v	volumetric concentration
I	intensity of light
M_{ox}	mixed molar mass of the oxidizer
M_{H_2O}	molar mass of water
$\dot{m}_{fuel}$	flow rate of fuel
$\dot{m}_{ox}$	flow rate of oxidizer
$\dot{m}_{wm}^{ox}$	flow rate of liquid water mist suspended in the oxidizer
$\dot{m}_{wm}^{mb}$	flow rate of water into the apparatus
ΔP_{ox}	differential pressure of oxidizer measured by the pitot probe
$\dot{Q}$	heat release rate
Q_i	mean extinction term
R	ideal gas constant
T	relative transmission
T_{ox}	temperature of oxidizer
$X_{H_2O}^{ox}$	concentration of water in the oxidizer
$X_{H_2O}^{\infty}$	concentration of water in the ambient air
Y_{wm}^{ox}	mass fraction of liquid water mist in the oxidizer stream
η_{comb}	combustion efficiency
ρ_{wm}	density of water mist
ρ_{ox}	density of oxidizer
v_i	relative volume
χ_{conv}	convective fraction of the combustion heat release rate
χ_{rad}	radiative loss fraction

Chapter 1: Introduction

1.1 Motivation

Fire suppression systems are an integral part of the built environment and provide a primary means of protecting life and property from fire hazards. The interactions between flames and water spray represent one of the essential interests of fire safety science due to the importance of water-based fire suppression systems, which are prevalent in modern construction, as the fire suppression performance of water is difficult to match. In addition, modern water-based fire suppression systems are extremely reliable when maintained in accordance with codes and standards. As governmental requirements for water-based fire suppression systems become more commonplace in occupancies ranging from high-rises to small residential communities and government restrictions on clean agents continue, the opportunities for design innovation grow exponentially. The market for a cost effective water-based fire suppression system that can protect life and property without causing damage in the form of the destructive capabilities of water, such as water mist, is great. However, these opportunities are restricted by an inability to accurately predict suppression performance in realistic configurations.

Prior work by a team of researchers at the University of Maryland has resulted in the development of a novel and canonical turbulent line burner facility proven to be capable of providing a buoyant, turbulent, methane-fueled diffusion flame suppressed via nitrogen dilution. The existing facility features well-characterized inlet and boundary conditions that are particularly useful in numerical simulations and non-

intrusive diagnostics to provide detailed measurements of suppression behavior to aid in the development and validation of advanced suppression models. Modifications to the apparatus are necessary to allow for the use of the turbulent line burner facility to evaluate suppression via fine water mist. The pursuit of this capability requires further research to attain a detailed understanding of the complex processes that govern fire suppression via water mist.

1.2 Literature Review

Traditional automatic fire suppression systems use water drops typically of a median drop size of approximately 750 µm to 1 mm [1] [2]. These systems deliver a far greater volume of water than that required to suppress a given fire [2]. Larger droplets pass through the flame zone without evaporating, therefore, the cooling capacity of large droplets is not completely utilized and a large amount of water remains as residue [2]. This literature review focuses on the advantages and characteristics of smaller droplet fire suppression systems typically identified as water mist systems.

1.2.1 Water Mist Characteristics

A water mist spray is constituted by a number of droplets, typically approximated as spheres. The spray presents a distribution of different values of diameter, each referring to a share of the total amount of droplets [3]. Characteristic drop size is typically expressed as d_{VF}, which is the representative diameter (d), where a fraction of the total sprayed volume (VF) consists of droplets having diameters smaller than the stated value [3].

National Fire Protection Association (NFPA) 750, *Standard on Water Mist Fire Protection Systems,* 2015 edition, defines a water mist as:

> *A water spray for which the* $Dv_{0.99}$, *for the flow-weighted cumulative volumetric distribution of water droplets is less than 1000 μm within the nozzle operating pressure range.*

However, water mist systems are more typically characterized by smaller (finer) droplets defined as those ranging from 10 to 100 μm in diameter [1] [2]. The fine water droplets that make up water mist are more effective than larger droplets due to their large surface area to volume ratio, resulting in rapid evaporation, faster cooling of hot gases, and longer suspension times in quiescent air, which combine to improve vaporization in the vicinity of the fire, requiring less water to accomplish extinguishment and minimizing water residue [1] [2]. In addition, small droplets are entrained more rapidly, follow the flow field of the combustion gases, and have the ability to reach obstructed areas in total flooding applications, providing maximum suppression for a minimum spray mass density [2] [5].

For low velocities of fuel and co-flowing air, it has been shown that water droplets evaporate well outside the flame and the resulting water vapor entrains into the flame with the air stream. The suppression effectiveness of water droplets is directly related to the proximity of the droplets to the flame as they evaporate, their flow dynamics and resulting water vapor entrainment [6]. Experimental results have shown that when monodisperse droplets are introduced with an air stream, there is an optimal droplet diameter (30 μm) that maximizes the flame extinction effectiveness, which is characterized by the extinction flow strain rate [7]. This optimal droplet

diameter is the threshold above which droplets cannot evaporate completely within the flame zone [2]. Ultra-fine water mist consists of extremely small water droplets (less than 30 µm) formed at atmospheric pressure using ultrasound vibration of piezoelectric discs similar to those used in commercial humidifiers [8]. Ultra-fine water mist droplets can follow fluid flow streamlines and reach behind obstructions due to very small inertia. The droplets do not wet surfaces significantly and may cause only minimal damage to electronics due to significant evaporation in dry air at ambient temperatures [8]. In addition, ultra-fine water mist droplets have large settling times due very low gravity effects, such that a high concentration of droplets may be suspended in air compared to traditional water mist formed by high pressure nozzles [8]. Extremely fine droplets on the order of 1 to 10 µm can also scatter and absorb the thermal radiation from a fire [8].

1.2.2 Development of Water Mist Technology

The development of water mist technology has been largely driven by the need to replace Halon 1301 (bromotrifluoromethane [CF_3Br]), a halogen-based suppression agent that adversely affects the ozone layer and has been banned from further production via the Montreal Protocol [2] [8]. Halon 1301 is a gaseous agent that readily diffuses and interacts chemically with the combustion process by interrupting chain-branching reactions that are critical to the propagation of combustion [8]. Water mist systems are considered a viable replacement for Halon 1301 and provide advantages over traditional sprinkler systems in that fine water droplets with relatively long settling times under normal gravity conditions can be an

4

excellent suppressant for gaseous fires in enclosures where total flooding is typically required [1] [9].

Water mist has also expanded from a halon replacement agent into traditional sprinkler applications [10]. In particular, for flammable liquid fires, water mist systems have demonstrated that they can deliver equivalent or better fire protection performance with less water usage [10]. In addition, smaller droplets are potentially easier to deliver, particularly around obstructions, and can be more effective than the larger drops (> 100 µm) currently in use in most fire suppression systems [11].

Despite its advantages, water mist fire suppression is complex and not well understood quantitatively, therefore, the fire protection industry relies primarily on an expensive, large-scale testing approach to develop water mist fire protection systems, making the further development of many potential applications cost prohibitive [10].

1.2.3 Suppression via Water Mist

Before exploring the mechanisms by which water mist suppresses, controls, and in some cases extinguishes a fire, it is important to understand the definitions of these terms. NFPA 750, *Standard on Water Mist Fire Protection Systems,* 2015 edition provides the following definitions:

- Fire Control: *Limiting the size of a fire by distribution of water so as to decrease the heat release rate and pre-wet adjacent combustibles, while controlling ceiling gas temperatures to avoid structural damage.*

- Fire Extinguishment: *The complete suppression of a fire until there are no burning combustibles.*

5

- Fire Suppression: *The sharp reduction of the rate of heat release of a fire and the prevention of regrowth.*

In order to suppress a fire burning with a continuous supply of fuel and oxygen, the suppressant must limit the fuel, limit the oxygen supply, or reduce the temperature of the flame zone. Fire suppression via water mist combines several physical phenomena, however, the primary mechanisms involved are gas phase cooling, oxygen dilution, fuel surface cooling and dilution, and radiation attenuation [5] [12].

Gas phase cooling occurs when a significant amount of heat is transferred from the combustion gases to the water mist droplets as they evaporate in or near the fire, forming water vapor (steam). The steam then absorbs additional heat as it is heated to the flame temperature, as its heat capacity is approximately twice that of air. The heat sink phenomena provided by the generation of steam results in a strong temperature decrease surrounding the flame and contributes to the reduction of the intensity of the combustion reactions [13] [14].

Next, oxygen dilution occurs during the phase change from liquid to vapor (evaporation), which induces a high volumetric expansion rate consisting of water vapor gas and prevents the mixing between fresh air and combustible vapor, acting like an inerting gas and further reducing the intensity of the combustion reactions [14]. In an enclosed space, the available oxygen is rapidly consumed by the fire and the steady flow of water mist evaporating to vapor, ultimately extinguishing the fire [13].

Fuel surface cooling occurs when fine droplets fall on the fuel surface and dissolve in the fuel, absorbing latent and/or sensible heat from the condensed fuel surface, diminishing the heat available for fuel gasification, reducing the rate of production of gaseous fuel, and changing the concentration of fuel evaporating from the fuel surface [5] [13]. As the condensed fuel gasification rate decreases, the heat release rate of the fire decreases [13]. Finally, if the droplets are small enough, they interact with the thermal radiation emitted by the fire by absorption and scattering effects, resulting in radiation attenuation [14].

Radiation attenuation occurs when the presence of water mist changes the net radiation reaching the fuel surface and affects the heat feedback to the fuel surface and reduces the fuel surface temperature [5]. The water mist ultimately acts as a radiative shield between the flames and the fuel surface [14]. The amount of attenuation is a function of droplet diameter and concentration [13]. For a given water volume, the finer the droplets, the greater the exchange surface between the droplets and the surroundings is, resulting in stronger evaporation effects [12].

As has been well reported in the literature, the distinction of which phenomena primarily contributes to suppression via water mist due is heavily configuration dependent and varies with several factors, including the droplet size distribution, the orientation of mist injection, and the velocity of the droplets relative to entrainment [8] [9] [11] [15-21]. For example, if droplets are too small or move too slowly, evaporation occurs too rapidly or too far upstream of the flame sheet. However, if droplets are too large or move too quickly, evaporation is too slow to affect significant flame cooling. Peak suppression performance and, therefore, the

minimum flame extinction limit is reached in configurations that achieve maximum droplet evaporation as close to the flame sheet as possible. At present, while it may be possible to predict peak suppression performance conditions for simplistic configurations with steady laminar flames, it is not possible to predict suppression performance for realistic configurations with turbulent flame-mist interactions. Table 1 provides both experimental measurements and numerical predictions of the minimum flame extinction limit from a range of configurations available in the literature investigating various fuel sources and mist characteristics. As shown, there is significant variation amongst the reported extinction limits, principally due to the sensitivity of water mist suppression performance to the peak suppression performance criteria.

Experimental studies that utilize small-scale laminar flames are useful in exploring extinction theory and establishing critical extinguishing limits for fuels, however, suppression in these studies is more characteristic of partially-premixed flames, than of the diffusion flames encountered in typical fire applications. It is not well understood how the extinguishment mechanisms observed in small-scale laminar flames relate to the suppression of larger-scale turbulent flames, where suppression is more commonly thought to result from extinction as a result of fuel surface cooling. The use of the novel and canonical turbulent line burner facility allows for the generation of water mist with low momentum to provide a steady, uniform, mist-laden oxidizer that is naturally entrained into the flame. This configuration allows for the investigation of natural suppression mechanisms in a buoyant, turbulent flame representative of realistic fire behavior, while still allowing for the detailed

8

characterization and controlled conditions necessary to provide insight into the

suppression mechanisms that dictate flame behaviors for conditions ranging from

complete combustion to partial and total extinguishment.

Table 1 Extinction Limits for Diffusion Flames Subjected to Water Mist

Source	Fuel	Configuration	Burner Type	Flow	Droplet Size (µm)	Y_{wm}^{ext}
[11]	Propane	Co-flow	Cup	Laminar	6.2 (d_{10})	0.125
[15]	Heptane	Co-Flow	Cup	Laminar	8.2 (d_{v50})	0.145
[21]	Methane	Counter-flow	Tsuji	Laminar	40-60 (d_{32})	0.090[a]
[22]	Heptane	Room Flooding	Pan	Turbulent	< 10	0.090
[19]	PMMA	Boundary Layer	Flat Plate	Laminar	3.2 (d_{32})	> 0.043
[16]	Methane	Co-flow	Slot	Laminar	50	0.175
[16]	Methane	Co-flow	Slot	Laminar	150	0.500
[8]	Propane	Co-flow	Cup	Laminar	4	0.150
[8]	Propane	Co-flow	Cup	Laminar	32	0.105
[20]	PMMA	Boundary Layer	Flat Plate	Laminar	6	0.095
[20]	PMMA	Boundary Layer	Flat Plate	Laminar	40	0.055
[20]	PMMA	Boundary Layer	Flat Plate	Laminar	100	0.135

1.3 Objective

As previously described, water has a high heat capacity and high latent heat of

evaporation that can absorb a significant quantity of heat from flames. In addition,

water expands approximately 1,700 times when it evaporates to vapor, resulting in the

dilution of the surrounding oxygen concentration. Fine water droplets increase the effectiveness of fire suppression due to the significant increase in the surface area of water available for heat absorption and evaporation [2].

Previous studies that have focused on water mist suppression have presented results that vary in suppression performance with changing spray characteristics [8] [9] [11] [15-21]. The consensus provided by these works is that water mist fire suppression systems are capable of successfully performing fire control and suppression in a large variety of fire scenarios, however, complete extinguishment is reached only in particular configurations, varying with factors including the droplet size distribution, the orientation of mist injection, and the velocity of the droplets relative to flame entrainment. Peak suppression performance occurs when droplets evaporate close to the flame sheet, maximizing latent cooling effects. Prior studies have concluded that very small droplets have low initial momentum, which reduces their ability to penetrate the flame zone [14]. Advanced modeling techniques are required to evaluate the complicated flows generated by water mist flooding in the fire environment [14].

Despite the progress that is apparent in the existing literature, most previous suppression studies are limited to simplistic configurations with small laminar flames and lack the diagnostics necessary to quantify suppression performance. Unlike laminar flames, turbulent flames offer additional features, including more intense radiative emissions, structural non-uniformity, and flame to flame interactions. It has not yet been demonstrated how or whether these features affect flame suppression behavior.

Recent applied studies investigating large-scale realistic configurations with turbulent flames have lacked the detailed characterization and controlled conditions necessary for model validation [12] [14] [22]. Visibly absent from the available literature, are studies employing a well-characterized configuration containing both the complexity required for relation to realistic fire scenarios and the detailed diagnostics required for contributions to the development and validation of computational fluid dynamics (CFD) models, where CFD tools represent the best available method of achieving predictive modeling of fire suppression performance. The existing turbulent line burner facility at the University of Maryland provides an opportunity to adapt the existing experimental facility for use in evaluating water mist fire suppression behaviors in a turbulent flame.

While a foundation of the water mist generation system was already in place for use with the turbulent line burner facility, additions and refinements to the control systems, measurement capabilities, and diagnostics were necessary to provide the well-characterized inlet conditions necessary for model validation and overall volume of water mist available for suppression. The primary deliverables for the present work include (1) the continued development of a well-characterized experimental facility for present and future studies of turbulent fire suppression phenomena; (2) the utilization of multiple non-intrusive diagnostics to provide insightful measurements of water mist suppressant-flame interactions and global suppression performance; (3) a database of measurements, including water mist characterization and turbulent flame temperature data made available to the general fire modeling community and suitable to support the development and validation of advanced fire suppression

models; and (4) the dissemination of these and other results of interest through scientific journal publications and conference proceedings.

The long-term goal of this work is the continued successful realization of performance-based design methods for fire suppression systems. The achievement of this objective would equip fire protection engineers with analytical design tools based on a fundamental understanding of suppression phenomena. These tools would provide a framework for evaluating suppression performance as a function of design input, enhancing design efficiency for standard applications while permitting the design of innovative solutions for exotic applications. The broader impact of this research would be the development of more cost-effective water mist fire suppression technologies while promoting improved life safety and infrastructure protection from fire.

Chapter 2: Approach

2.1 Overview

The primary objective of the this work is to provide a detailed experimental study of water mist fire suppression phenomena in a buoyant, turbulent diffusion flame representing the key characteristics of a realistic fire. The experimental configuration features an existing laboratory scale facility that has been proven to provide well-characterized inlet and boundary conditions suitable for application to CFD fire simulations for nitrogen-based suppression experiments, wherein the facility was modified to allow for the use of water mist, while still taking advantage of the existing classical species-based calorimetry techniques the facility provides to quantify water mist suppression performance.

In addition, a secondary objective of this work is to collect turbulent flame temperature data, such that future work can accurately determine the interaction of the water mist with the flame. The primary goal of this work is to provide a detailed dataset suitable to support the development and validation of predictive fire suppression models.

The experiments feature an experimental apparatus built upon the facility developed by White et al. [23] [24], and uses a slot burner flowing a gaseous fuel to provide a low-strain, buoyant, turbulent diffusion flame in a line-fire configuration. Water mist is provided via a co-flowing oxidizer stream, and the primary means of flame suppression is thermal quenching due to a combination of oxidizer dilution and evaporative cooling.

13

Current measurement capabilities include flame imaging, flame temperature fluctuations, water mist mass loading, water mist droplet size distribution and density, as well as calorimetry techniques to measure flame heat release rate and combustion efficiency.

2.2 Configuration

2.2.1 Burner and Flame

The experimental apparatus was built upon the facility developed by White et al. [23] [24], and uses a slot burner flowing a gaseous fuel to provide a low-strain, buoyant, turbulent diffusion flame in a line-fire configuration. As detailed by White [25], the dimensions of the burner and the fuel mass flow rates were selected to ensure the flames meet the line-fire, buoyancy, and turbulence constraints. The full import of these constraints are detailed by White [25], and are summarized, as follows:

- The line-fire constraint limits the mean flame height relative to the burner length, while also limiting the aspect ratio such that three-dimensional edge effects are minimized in the flame.
- The buoyancy constraint is characterized by a fire-source Froude number that is less than a critical value that defines the transition from buoyancy-drive to momentum-dominated flow regimes.
- The turbulence constraint is characterized by a fire-source Grashof number evaluated at one-tenth of the flame height that is greater than

the critical value that defines the transition from laminar to fully turbulent flow regimes.

Based on the above constraints, a stainless steel slot burner 50 cm long by 5 cm wide by 7 cm tall with 1.5 mm thick side walls was utilized. Methane fuel of 99.9% purity was utilized for the experiments at a flow rate of 1 ± 0.02 g/s, equating to an approximately 50 kW flame. Previous analysis [25] has indicated that for Methane (CH_4), a fuel flow rate ($\dot{m}_{fuel}$) of approximately 1 g/s sufficiently satisfies the buoyancy and turbulence constraints.

Outside the apparatus, fuel is supplied to the burner from a pressurized cylinder through a 7.5 m length of 6.4 mm outer diameter copper tubing. The fuel passes through a mass flow controller and then enters the burner at the bottom of a 2 cm tall plenum space, then filters through a 5 cm tall bed of ground glass to facilitate uniform fuel delivery. An exposed-junction K-type thermocouple probe positioned at the center of the fuel port provides a measurement of the fuel inlet temperature with an uncertainty of ± 2 K and a response time of approximate 3 s. Surrounding the burner rim is a thin, 5 cm wide strip of ceramic fiberboard, which promotes horizontally directed entrainment at the flame base and has been shown in previous work to promote transition to fully turbulent flame conditions [23]. A schematic depicting the main experimental apparatus is provided in Figure 1. The resultant flame transitions from laminar to turbulent at approximately 2.7 cm above the burner.
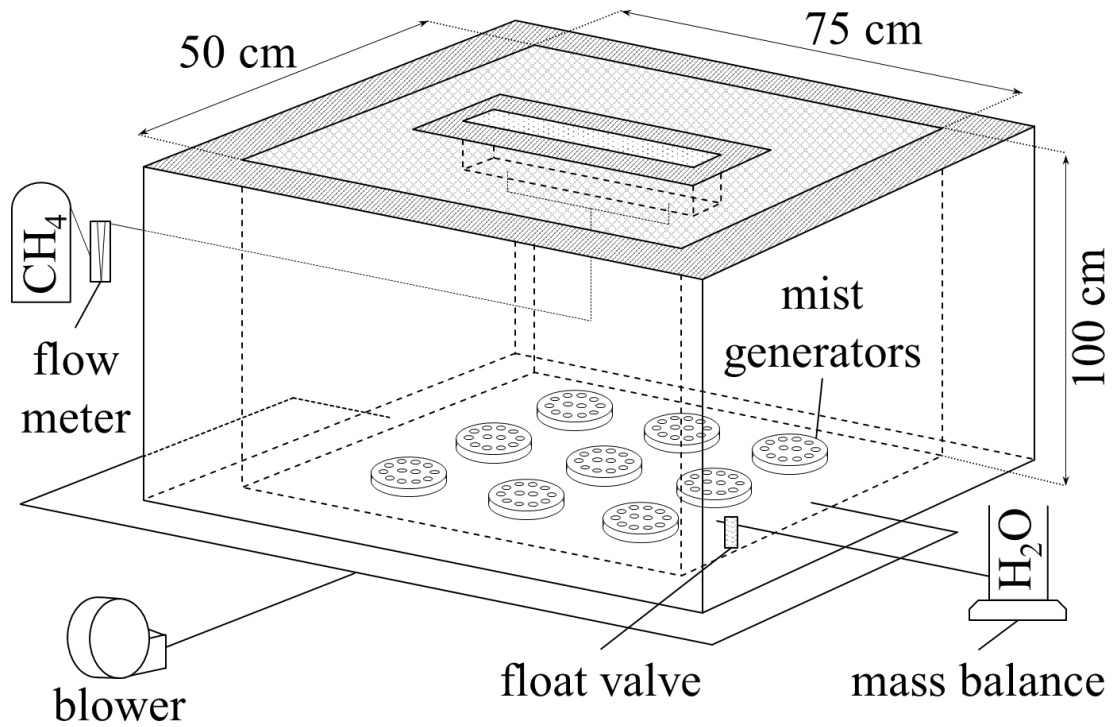
Figure 1 Turbulent Line Burner Apparatus

Although not strictly part of the current experimental work, the design of the turbulent line burner apparatus is such that it lends itself to the controlled measurement of turbulent flame gas phase temperatures using high response time ultra-fine wire thermocouple probes to reduce radiative effects. A structure was constructed above the surface of the oxidizer port to allow the mounting of four (4) micro thermocouples such that their height and position above the surface of the burner is adjustable, as shown in Figure 2.

The micro thermocouple probes each consist of type S, Platinum / Rhodium, ultra-fine wire thermocouples 12.7 µm in diameter capable of a 5 millisecond response time, wrapped in an inconel sheath. Type S thermocouples are capable of measuring temperatures up to 2041 K.
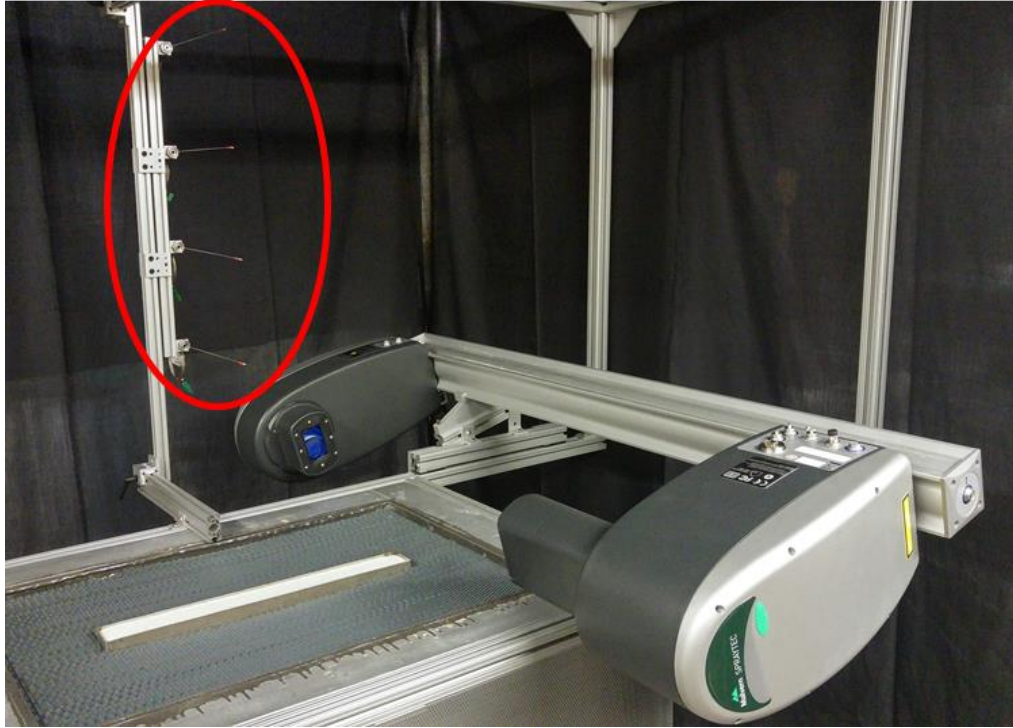
Figure 2 Thermocouple structure and mounting above the surface of the burner (circled in red)

2.2.2 Co-flowing Oxidizer

Surrounding the burner is an apparatus designed to produce a controlled, uniform co-flowing oxidizer, with the ability to deliver various suppressants to the flame. The oxidizer is intended to minimally impact the entrainment structure of the flame, while also shielding the flame from significant interaction with ambient air, thereby ensuring that the flame interacts primarily with the suppressant-laden environment provided by the oxidizer. As such, the dimensions of the oxidizer apparatus and the oxidizer mass flow rates were selected to ensure the oxidizer meets the flame-interaction and ambient-occlusion constraints.

The oxidizer apparatus comprises a sealed rectangular structure with internal dimensions 50 cm wide by 75 cm long by 100 cm tall. Oxidizer enters at the base of the structure, mixing within the internal volume before passing through a 7.6 cm thick aluminum honeycomb of 9.5 mm hexagonal cells. The honeycomb defines the oxidizer port at the top of the structure, conditioning the flow with a uniform vertical velocity profile while still allowing the mist droplets to pass through the cells without significant water losses due to the trapping of droplets inside the honeycomb. The oxidizer port sits 15 mm below the fuel port, while the 10 cm wide perimeter of the oxidizer apparatus sits at the same elevation as the fuel port. A plan view of the oxidizer port surface is provided in Figure 3.

Figure 3 Plan view of oxidizer port surface

18

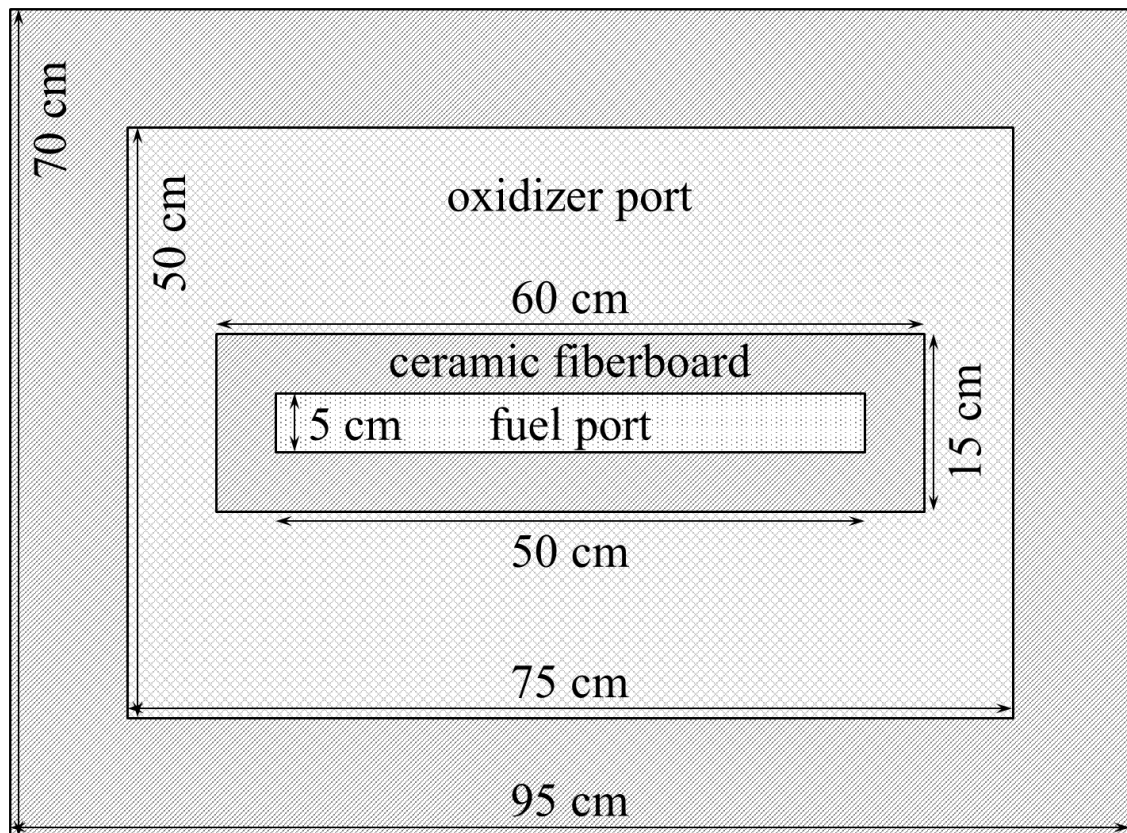Air for the oxidizer is supplied by an electric centrifugal blower through 8.9 cm outer diameter piping, with the flow rate controlled by a manual gate valve and measured using a United Sensor pitot-static probe connected to a Setra Model 264 differential pressure transducer. Sufficient lengths of straight piping are provided upstream and downstream of the pitot probe to ensure fully-developed flow and promote measurement stability. However, the length of pipe is reduced in the present work to reduce friction losses previously noted in the oxidizer delivery system, allowing increased oxidizer flow.

The flow rate measured by the calibrated pitot probe is determined by:

$$\dot{m}_{ox} = C_f^{ox} A_{ox} \left(\frac{2 \Delta P_{ox} P_{ox} M_{ox}}{R T_{ox}} \right)^{1/2} \tag{1}$$

where ΔP_{ox} is the differential pressure measured by the pitot probe, M_{ox} is the mixed molar mass of the oxidizer, R is the ideal gas constant, T_{ox} is the temperature of the oxidizer, and C_f^{ox} is a flow coefficient characterizing the velocity distribution across the cross sectional area (A_{ox}). Bernoulli's principle is further applied to relate the measured differential pressure to the flow velocity, which is related to the mass flow rate via the flow density using the ideal gas law. Prior work [25] provided a typical calibration curve for the pitot probe that defined $C_f^{ox} = 0.8972$ for the present work.

2.2.3 Water Mist Suppression

Water mist for flame suppression is produced using an array of nine model DK12-36 ultrasonic mist generators, submerged in a 7 cm deep layer of water within the base of the apparatus (see Figure 1), arranged as shown in Figure 4. Each mist

generator includes twelve individual 20 mm diameter piezoelectric atomizers, which

vibrate at ultrasonic frequency to produce a plume of fine mist droplets just above the

water surface.
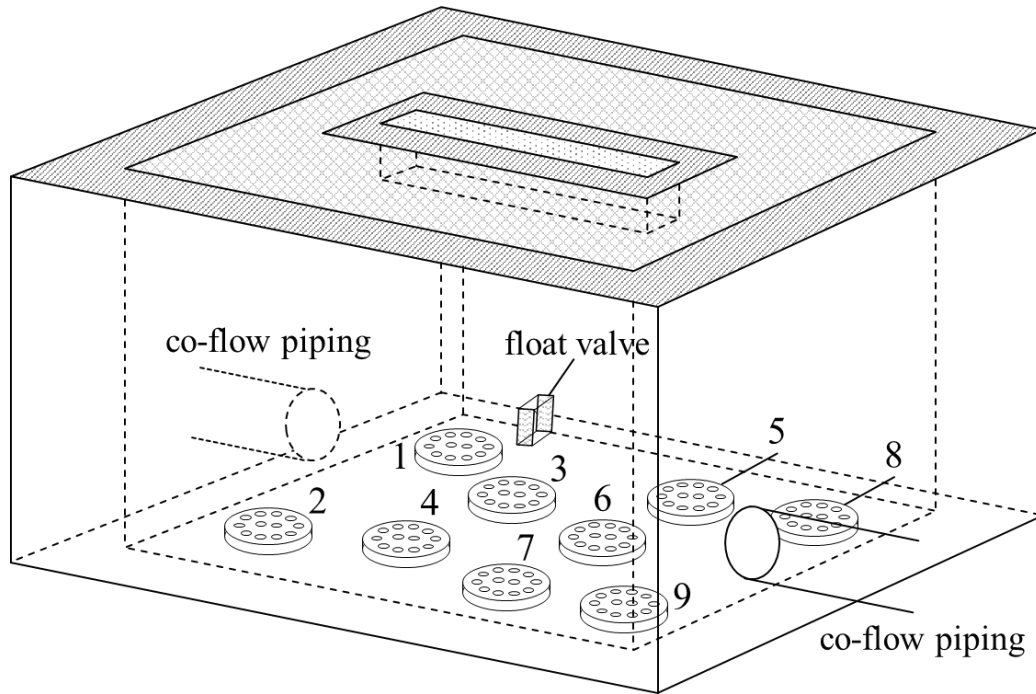
Figure 4 Actual test arrangement of water mist generators

Water is supplied from an open-top container located 1.4 m above the base of

the apparatus. The container is positioned on a calibrated Mettler Toledo mass

balance (Model MS32001L; uncertainty 0.1 g; response time 2 s), which is used to

measure the flow rate of water into the facility. Water flows due to gravity from the

container to the apparatus through a short length of 6 mm outer diameter flexible

tubing. Proper maintenance of water level is a primary factor in the mist generation

efficiency of the atomizers, therefore, the water level inside the existing apparatus

was adjusted by the addition of a flat metal plate at the bottom of the water basin that

20

the atomizers rest upon, which allows for the precise amount of water above the atomizers required to generate the maximum amount of water mist. This water level is maintained using a float control valve that closes once a specified depth is reached, and reopens when the water level begins to recede. For steady-state conditions, the inward flow rate of water measured using the mass balance is approximately equal to the flow rate of mist produced by the generators.

As previously described, air for the co-flowing oxidizer is supplied at a constant rate from an electric centrifugal blower, measured using a calibrated pitot-static probe, and delivered to the base of the apparatus through 8.9 cm outer diameter piping. Inside the apparatus, this piping is redistributed to provide a downward flow of air across the water surface, supporting uniform mixing of the air with the mist. The mist is entrained upward by the flowing air, passing through the aluminum honeycomb, which ensures a uniform distribution of mist-laden air at the outlet of the oxidizer port. A mist containment system consisting of a 1.2 m long fiberglass curtain is suspended from the hood above the experimental apparatus, allowing for a homogenized mist condition if the flame region. A full description of the water mist characterization is provided in Section 2.3.

2.2.4 Calorimetry

The experimental apparatus is centrally positioned roughly 1.1 m beneath a 2 m by 2 m hood connected to an exhaust evacuation system that uses perforated plates to block a separate inlet outside the experimental apparatus, allowing an exhaust flow of roughly 1 kg/s, measured using a Veris Verabar V100 averaging pitot tube (uncertainty 1%), inside the confines of the experimental hood. This increased

21

exhaust flow improves the distribution of water mist in the flame region and reduces secondary flows.

As previously described, a 1.2 m long fiberglass curtain is suspended around the perimeter of the hood, encasing the experimental facility in a mist containment system. This curtain further distributes the suction of the exhaust system around the apparatus, yielding a background upward flow of roughly 25 cm/s, sufficient to suspend droplets with diameter less than 90 mm in free fall, encouraging entrainment of the mist upward into the flame, and preventing accumulation of droplets around the flame base. The curtain additionally shields the flame and oxidizer from air currents in the outer ambient and ensures total capture of all mist and combustion products into the exhaust system.

Within the exhaust system, a gas sampling system provides for the measurement of the molar concentrations of the combustion products (O_2, CO_2, CO, and H_2O) in the exhaust stream. From these measurements, integral heat release rate (uncertainty 1.5 kW; response time 5 s) is derived via a novel implementation of mass conservation analyses coupled with classical species-based calorimetry techniques (for a detailed description of this measurement and associated instrumentation, see the prior work by White [25]).

2.3 Water Mist Characterization

As previously described, water mist for flame suppression is produced using an array of nine model DK12-36 ultrasonic mist generators, submerged in a 7 cm deep layer of water within the base of the apparatus (see Figure 1). Each mist generator includes twelve (12) individual 20 mm diameter piezoelectric atomizers, which

22

vibrate at ultrasonic frequency to produce a plume of fine mist droplets just above the surface of the water.

Multiple adjustments in the control system were made to the existing turbulent line burner facility to allow for increased water mist generation efficiency, as described previously, including streamlining of the oxidizer delivery system to reduce friction losses and increase oxidizer flow, water level improvements to increase mist generation efficiency, the addition of a larger honeycomb at the top of the oxidizer to allow water mist droplets to pass through while still serving as a flow straightener, the addition of a mist containment system to homogenize the water mist in the flame region, and increased exhaust flow inside the containment system to further improve the water mist distribution in the flame region and to reduce secondary flows. Following these improvements, the capabilities of the water mist generation system were characterized both using a classical mass balance approach and using more modern diagnostic techniques.

Prior work in the development of the turbulent line burner facility has noted that for a 50 kW flame, as utilized in the present work, the characteristic buoyant velocity scale for the flame is approximately 3 m/s. Further, the flame-interaction constraint requires that the velocity of the co-flowing oxidizer be less than one-tenth of the velocity of the flame, or approximately 30 cm/s, to allow for natural entrainment. In order for droplets to be carried by the co-flowing oxidizer, the drops must have a diameter of less than 53 µm [25]. An exhaust flow of 1 kg/s (25 cm/s) was added within the containment system to provide additional lift to the water mist, while remaining sufficiently smaller than the characteristic velocity of the flame,

encouraging entrainment of the water mist upward and into the flame, and preventing

the accumulation and roll over of droplets at the top of the oxidizer port.

2.3.1 Mass Fraction of Water Mist

The mass fraction of water mist in the oxidizer was characterized first using a

classical mass balance approach. The suppression potential of the oxidizer is

primarily characterized by the mass fraction of liquid water mist in the oxidizer

stream, which is defined as:

$$Y_{wm}^{ox} = \frac{\dot{m}_{wm}^{ox}}{\dot{m}_{ox} + \dot{m}_{wm}^{ox}} \tag{2}$$

where $\dot{m}_{ox}$ is the flow rate of the oxidizer and $\dot{m}_{wm}^{ox}$ is the flow rate of liquid water

mist suspended in the oxidizer, as determined from $\dot{m}_{wm}^{mb}$ using:

$$\dot{m}_{wm}^{ox} = \dot{m}_{wm}^{mb} - (X_{H_2O}^{ox} - X_{H_2O}^{\infty})\dot{m}_{ox}\frac{M_{H_2O}}{M_{ox}} \tag{3}$$

where M_{ox} is the mixed molar mass of the oxidizer (assumed to be a mixture of

ambient air and excess water vapor), M_{H_2O} is the molar mass of water, $X_{H_2O}^{ox}$ is the

concentration of water in the oxidizer, and $X_{H_2O}^{\infty}$ is the concentration of water in the

ambient air. Note that the second term in Equation (3) accounts for the fraction of

generated mist that evaporates before reaching the outlet of the oxidizer port.

During the actual suppression tests, the concentration of water in the oxidizer

(quantity $X_{H_2O}^{ox}$) was measured using a Michell Instruments PCMini52 humidity

sensor (uncertainty ±1% relative humidity; response time approximately 10 s)

mounted to the interior of the oxidizer port. The measured relative humidity is

related to $X_{H_2O}^{ox}$ via a thermodynamic state equation for the saturation pressure of

water vapor as a function of temperature [26]. For all tested conditions with mist

generation, $X_{H_2O}^{ox}$ is approximately equal to 0.027 (100% relative humidity).

Water was supplied from an open-top container located 1.4 m above the base of

the apparatus. The container was positioned on a calibrated Mettler Toledo mass

balance (Model MS32001L; uncertainty 0.1 g; response time 2 s), which was used to

measure the flow rate of water into the facility. Water flowed from the container to

the apparatus through a short length of 6 mm outer diameter flexible tubing, driven by

gravity. Proper maintenance of water level is a primary factor in the mist generation

efficiency of the atomizers, therefore, the water level inside the apparatus was

precisely maintained using a float control valve that closed once a specified depth

was reached, and reopened when the water level began to recede. Additionally, for

steady-state conditions, the inward flow rate of water measured using the mass

balance is approximately equal to the flow rate of mist produced by the generators.

Air for the co-flowing oxidizer is supplied at a constant rate from an electric

centrifugal blower, measured using a calibrated pitot-static probe, and delivered to the

base of the apparatus through 8.9 cm outer diameter piping. Inside the apparatus, this

piping is redistributed to provide a downward flow of air across the water surface,

supporting uniform mixing of the air with the mist. The mist is entrained upward by

the flowing air, passing through a 7.6 cm thick aluminum honeycomb with 9.5 mm

cells, which ensures a uniform distribution of mist-laden air at the outlet of the

oxidizer port. The mist configuration implemented in the present work has the

benefit of providing a well-characterized boundary condition featuring a steady and

uniform mist-laden oxidizer with low injection momentum that is naturally entrained into the flame.

As provided in the literature review, prior studies have shown that extinction via water mist occurs at concentrations of approximately 10% water in air. The capabilities of the test apparatus were characterized using this mass balance approach by varying the velocity of the co-flowing oxidizer supplied. As shown in Figure 5, an increase in the oxidizer flow rate resulted in an approximately linear increase in the water mist mass flow rate. However, as shown in Figure 6, the piezoelectric mist generators were not able to keep pace with the increase in oxidizer flow rate, such that the mist mass fraction decreased linearly with increased oxidizer flow. Images of the maximum water mist mass loading at each characterized oxidizer flow rate are provided in Figure 7.
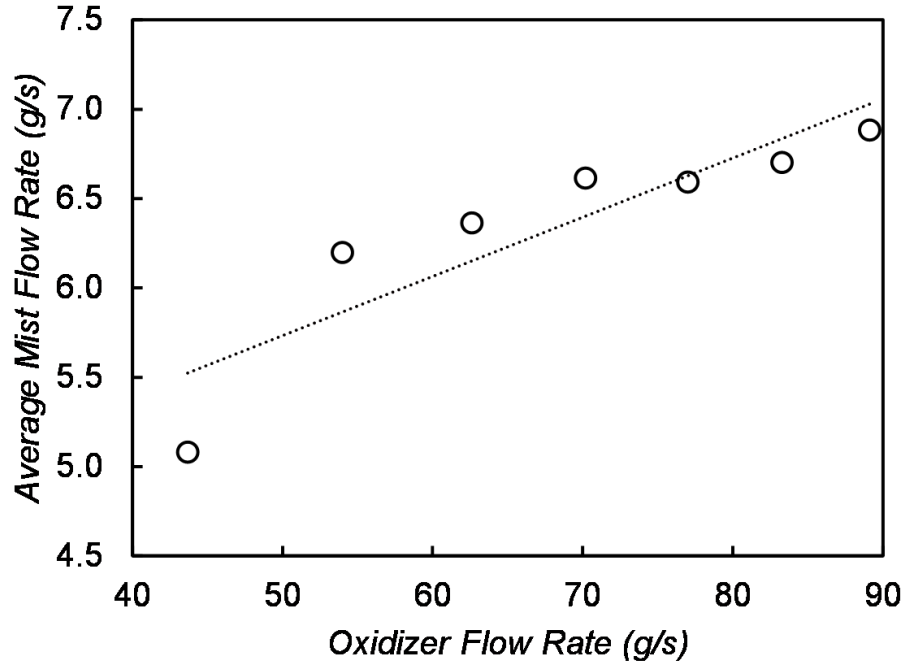
Figure 5 Average water mist mass flow rate as a function of the oxidizer flow rate
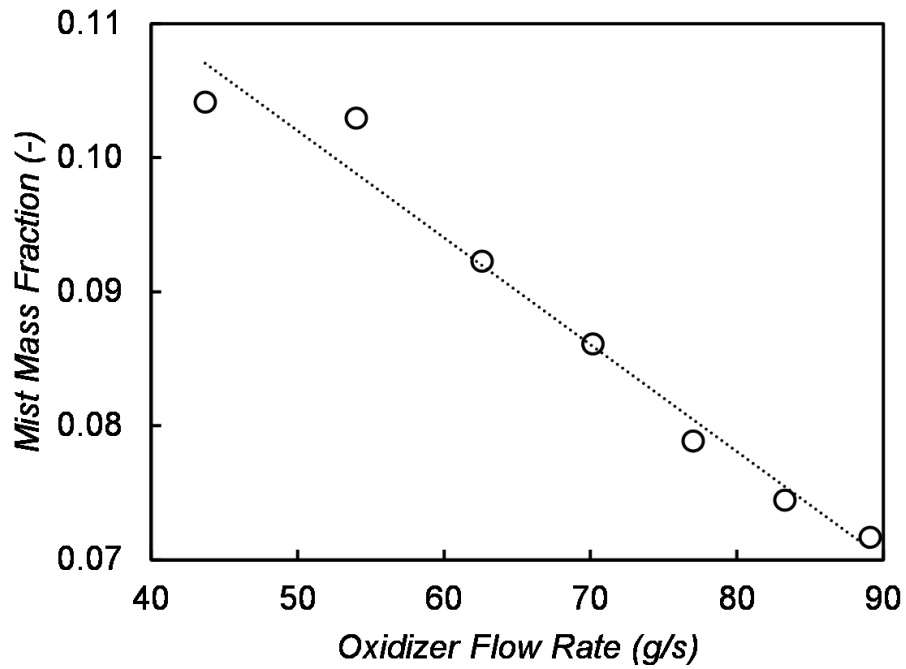
Figure 6 Water mist mass loading as a function of the oxidizer flow rate
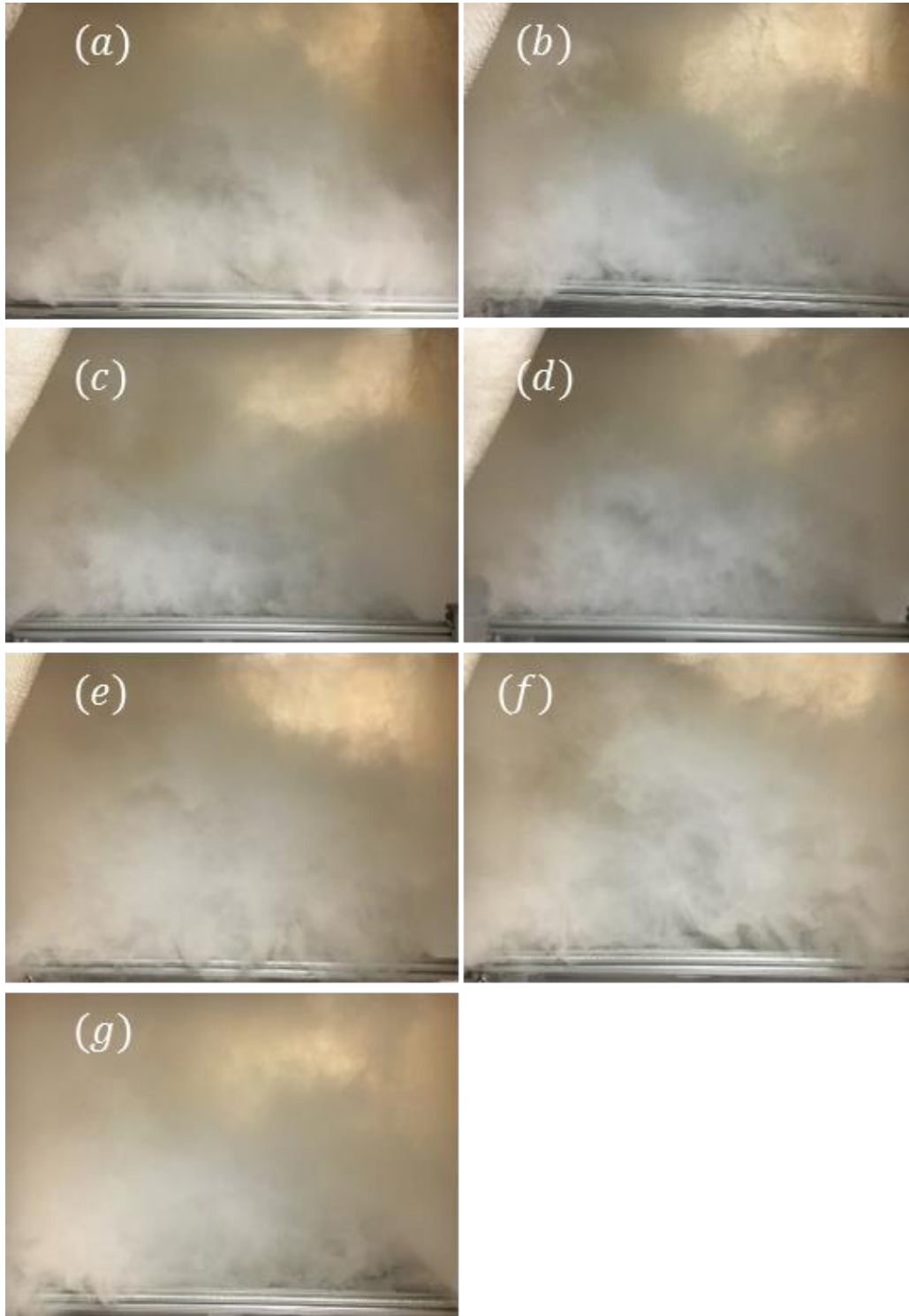
Figure 7 Images of water mist mass loading at varying oxidizer flow rates: (a) $\dot{m}_{ox}$ = 44 g/s and Y_{wm}^{ox} = 0.104; (b) $\dot{m}_{ox}$ = 54 g/s and Y_{wm}^{ox} = 0.103; (c) $\dot{m}_{ox}$ = 63 g/s and Y_{wm}^{ox} = 0.092; (d) $\dot{m}_{ox}$ = 70 g/s and Y_{wm}^{ox} = 0.086; (e) $\dot{m}_{ox}$ = 77 g/s and Y_{wm}^{ox} = 0.079; (f) $\dot{m}_{ox}$ = 83 g/s and Y_{wm}^{ox} = 0.074; (g) $\dot{m}_{ox}$ = 89 g/s and Y_{wm}^{ox} = 0.072

Although the lowest oxidizer flow rate (44 g/s or 13 cm/s) resulted in the highest water mist mass fraction ($Y_{wm}^{ox} = 0.104$), based on visual inspection, it was determined that a slightly higher oxidizer flow rate (54 g/s or 16 cm/s) better lifted the water mist to encourage interaction with the flame without compromising the mass loading ($Y_{wm}^{ox} = 0.103$). This oxidizer flow rate also satisfies the flame-interaction constraint, as provided in Section 2.3.

The available water mist mass loading was also characterized based on the number of mist generators engaged while the oxidizer flow rate was held steady at approximately 54 g/s (16 cm/s), such that the water mist mass loading could be varied during the calorimetry tests. As expected, the water mist mass fraction increased approximately linearly with each generator added (see Figure 8). Images of the maximum water mist mass loading for each number of generators are provided in Figure 9. A black plate was placed over the burner in each image to better visualize the density changes in the mist. Note that there is an inherent instability in the water mist mass loading that changes the mass fraction observed within a level of certainty, resulting in slightly different measurements between tests.
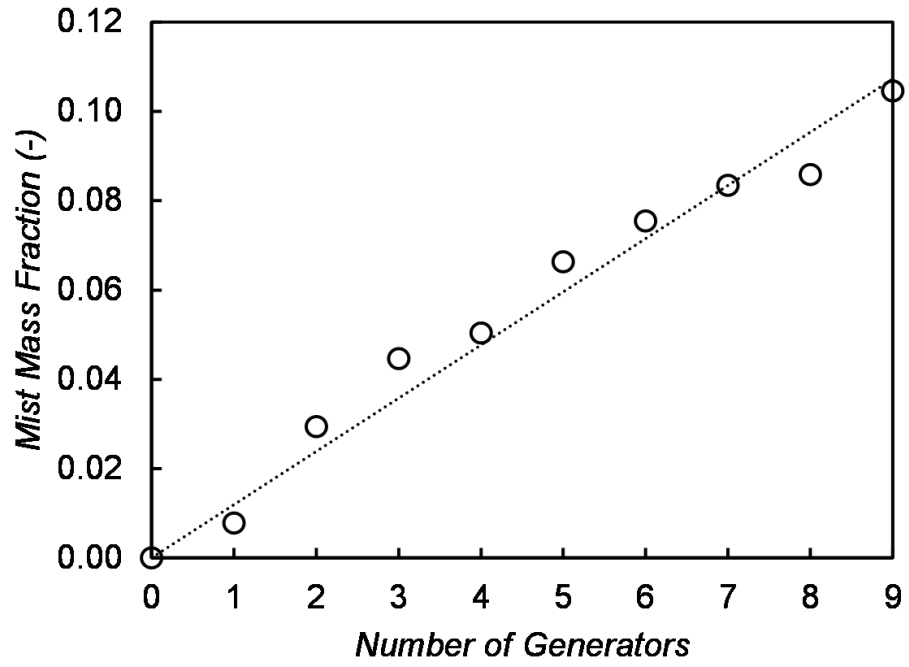
Figure 8 Water mist mass loading as a function of the number of generators engaged
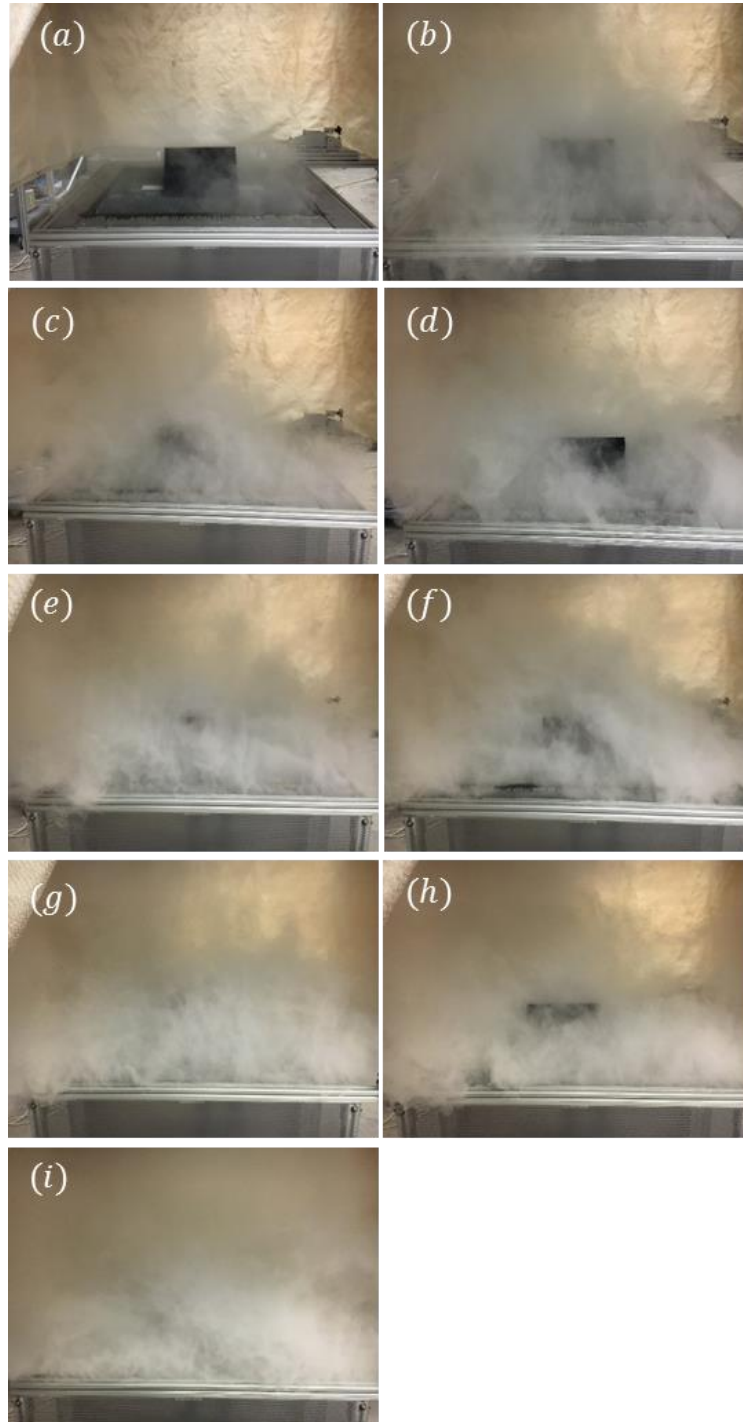
Figure 9 Images of water mist mass loading for each number of generators: (a) Generators = 1 and Y_{wm}^{ox} = 0.008; (b) Generators = 2 and Y_{wm}^{ox} = 0.029; (c) Generators = 3 and Y_{wm}^{ox} = 0.045; (d) Generators = 4 and Y_{wm}^{ox} = 0.050; (e) Generators = 5 and Y_{wm}^{ox} = 0.066; (f) Generators = 6 and Y_{wm}^{ox} = 0.075; (g) Generators = 7 and Y_{wm}^{ox} = 0.083; (h) Generators = 8 and Y_{wm}^{ox} = 0.086; (i) Generators = 9 and Y_{wm}^{ox} = 0.105

2.3.2 Droplet Size Distribution

The mist droplet size distribution was measured using a Malvern Instruments Spraytec system via laser diffraction technique, for which a collimated Helium-Neon laser beam (632.8 nm) is passed from the transmitter module, through the mist, to the receiver module. A multifaceted ring detector in the receiver module collects and analyzes the resulting light diffraction patterns produced by the mist as it passes through the laser. The Spraytec system uses Mie theory to determine particle size, which states that each size of particle has its own characteristic scattering pattern. The Spraytec detector array is made up of over 30 individual detectors, each of which collects the light scattered by a particular range of angles and assigns it to a data channel. Based on Mie theory, the angle at which a particle diffracts light is inversely proportional to its size, therefore, determining the angle of diffraction reveals the size of the droplet. The diffraction pattern signals are processed by analog and digital electronics boards, then passed to the analysis software, where the diffraction pattern is analyzed using an appropriate scattering model to calculate the spray size distribution. The Spraytec system resolves droplet diameters in a range between 0.1 and 900 µm (d_{v50} between 0.5 and 600 µm) with a measurement accuracy of ±1%. This accuracy is retained across a wide range of mist concentrations, permitting up to 95% obscuration of the laser.

For the present configuration, the Spraytec system was positioned such that the laser passed directly above the oxidizer port, without intersecting the space above the fuel port or ceramic fiberboard, as shown in Figure 10 and Figure 11. The Spraytec system was mounted on a sliding rail system such that the instrument could be

smoothly transitioned along a lateral profile to collect uniformity measurements. The

beam path length was controlled to provide total laser obscuration within the accuracy

limitations of the instrument.
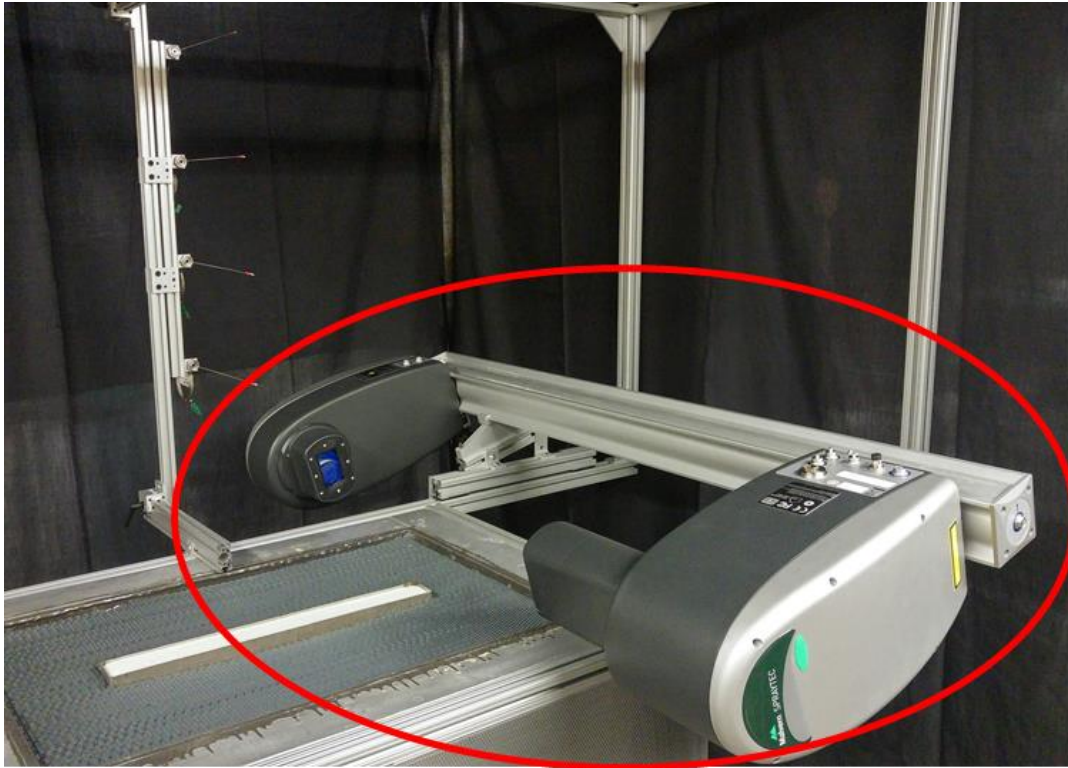
Figure 10 Malvern Instruments Spraytec system mounted to the apparatus
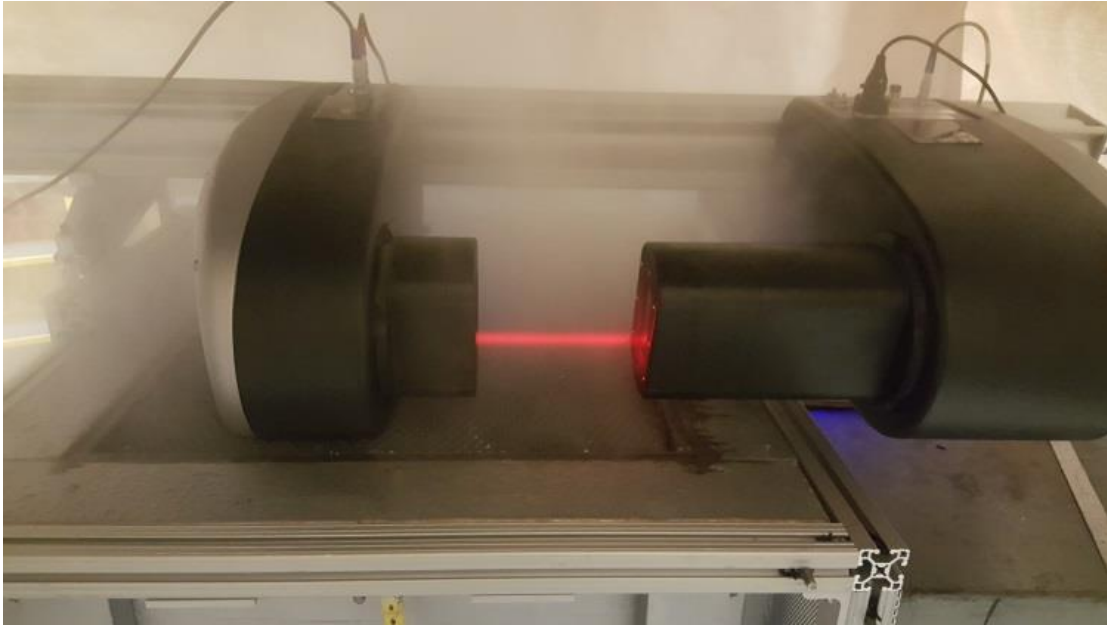
Figure 11 Spraytec system positioning above oxidizer port with one generator active

A typical droplet size distribution measured using the Spraytec system is presented in Figure 12. As shown, mist droplets in the present facility range primarily between 3 and 20 µm in diameter, with a Sauter mean diameter (d_{32}) of roughly 6.6 µm. For this size distribution, the characteristic spray surface area is roughly 0.9 m^2/cm^3. Additional droplet size statistics are reported in Table 2. The droplet size measurements exhibit an expected log-normal distribution, with an elongated upper tail between 50 and 100 mm, attributed to droplet coalescence.
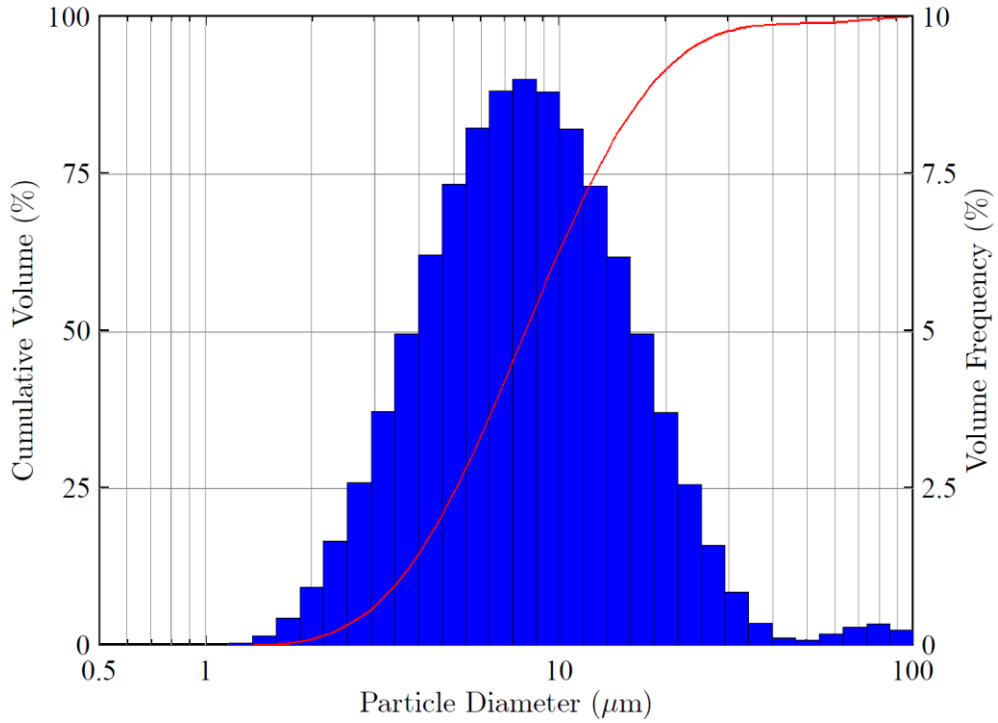
Figure 12 Spraytec measured droplet size distribution of water mist entrained with co-flowing oxidizer

Table 2 Spraytec measured droplet size statistics for mist entrained with co-flowing oxidizer

Parameter	Value (μm)
d_{v10}	3.5 ± 0.1
d_{v50}	8.0 ± 0.2
d_{v90}	18.8 ± 0.9
d_{32}	6.6 ± 0.1
d_{43}	10.4 ± 0.4

2.3.3 Volumetric Mist Concentration

In addition to evaluating the droplet size distribution from the beam scattering

patterns, the Spraytec system was also used to evaluate the volumetric mist

concentration measured from the obscuration of the laser through the mist and

calculated from the Beer-Lambert law:

$$\frac{I}{I_0} = e^{-\alpha b}$$

(4)

where I is the intensity of light at a distance (b) in the particle field of absorbance (α)

and I_0 is the intensity of the light beam as it enters the particle field. The quantity $\frac{I}{I_0}$

is the relative transmission (T) of the beam, measured directly by the Spraytec

system.

The volumetric concentration (C_v) is related to the relative transmission of the

beam measured directly by the Spraytec system using the following equation:

$$C_v = \frac{-2000\ln(T)}{3b \sum \frac{Q_i v_i}{d_i}}$$

(5)

where the particle size distribution (v_i) is the relative volume with mean diameter

(d_i), and the mean extinction term (Q_i) is calculated from scattering theory and is a

function of the optical properties of the particle and dispersant media.

The volumetric concentration is related to Y_{wm}^{ox} via

$$Y_{wm}^{ox} = \frac{C_v \rho_{wm}}{(1 - C_v)\rho_{ox} + C_v \rho_{wm}}$$

(6)

where ρ_{wm} is the density of the water mist and ρ_{ox} is the density of the oxidizer.

In order to collect the measurements, the Spraytec instrument was positioned

with the transmitter and receiver positioned such that the beam length was

approximately 150 mm. In addition, tubes were attached to both the transmitter and

receiver elements such that the measurement path was narrowed. To prevent the fine

mist from entering the tubes and obscuring the beam completely, a glass slide was placed over the end of each tube. The Spraytec measurements were evaluated using Equation (6) and compared to the classical mass balance approach described in Section 2.3.1 and were generally found to show good agreement with Y_{wm}^{ox} evaluated using Equations (1) and (2) with the mass balance measured $\dot{m}_{wm}^{mb}$ (within $\pm 10\%$), as shown in Figure 13. Note that while this work confirms that the Spraytec system is capable of measuring an accurate volumetric concentration in a dense mist, the measurements were not without issue and the repeatability under the same set of variables is questionable.
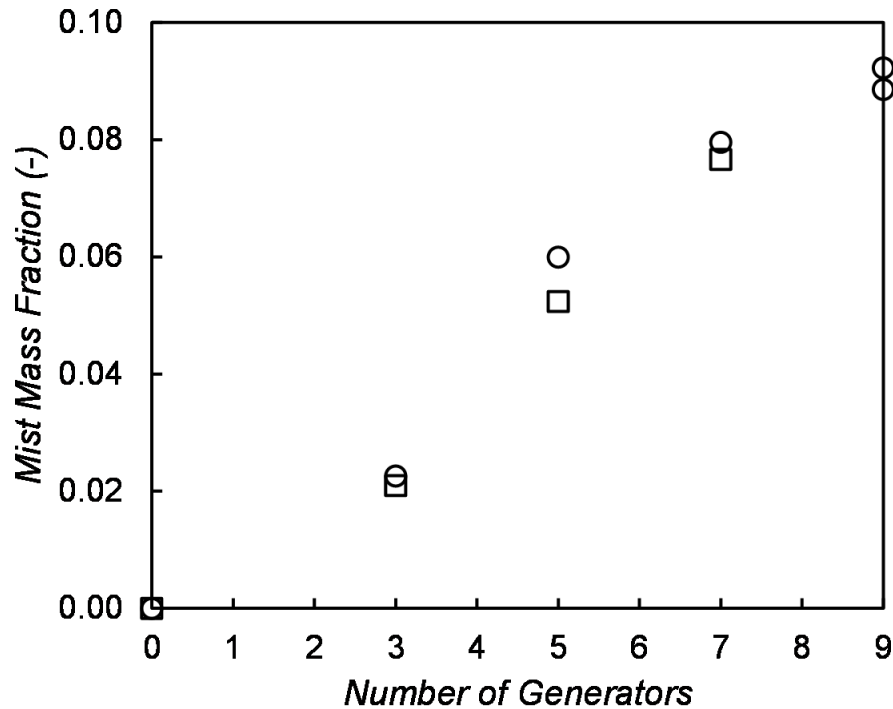
Figure 13 Comparison of mist mass fraction for varying number of generators using experimental (noted as circles) and Spraytec (noted as squares) methods of measurement

Steady-state Spraytec measurements were also recorded at incremental locations across the surface of the oxidizer port as shown in Figure 14. These measurements verify that the mist-laden oxidizer is sufficiently uniform, with combined spatial and temporal variations of less than $\pm$ 2% in the measured d_{32} and $\pm$ 5% in the C_v-derived Y_{wm}^{ox}, as shown in Figure 15.
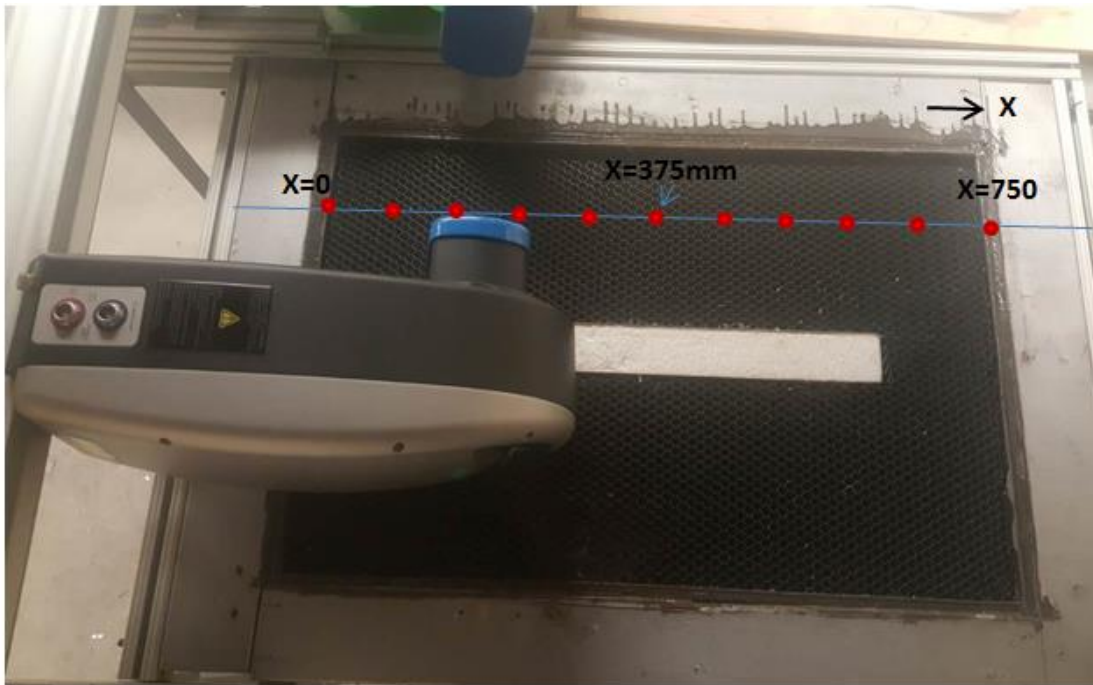
Figure 14 Steady-state measurement locations across the oxidizer port
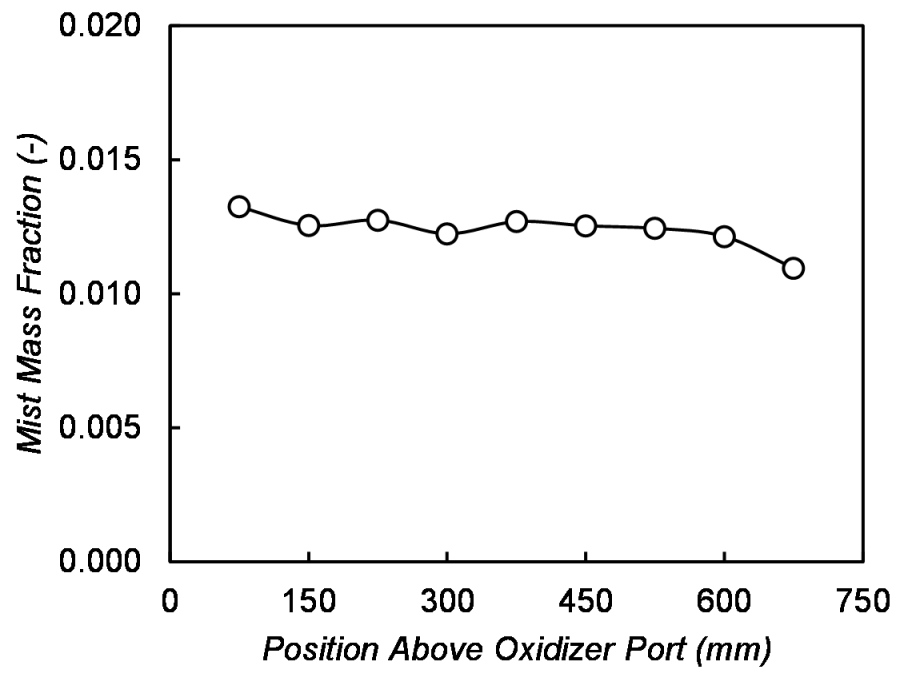
Figure 15 Steady-state water mist measurements across the oxidizer port; one generator active

2.4 Method of Tests

2.4.1 Suppression Tests

Five (5) total tests were conducted, each varying the water mist mass fraction based on the characterization tests, as shown in the test matrix presented in Table 3. The same test methodology was followed for each test:

1. Set oxidizer flow rate and allow to stabilize.

2. Set exhaust flow rate and allow to stabilize.

3. Begin data acquisition.

4. Ignite flame and let stabilize at 50 kW for 5 minutes.

5. Open water valve to allow on-demand filling of reservoir.

6. Initiate generators.

7. Allow generators to run for 15 minutes or until the flame is extinguished.

8. Shut off generators, flame, and close valve.

9. Stop data and reset for the next test.

Table 3 Test Matrix

Test Number	Number of Generators	Expected Mist Mass Fraction	Generator Arrangement
1	0	0	
2	3	0.045	
3	5	0.066	
4	7	0.083	
5	9	0.105	

2.4.2 Temperature Measurements

Tests were conducted to evaluate the vertical centerline and cross-flame profiles of the time-mean gas temperatures. For the cross-flame profile, fourteen (14) total measurement points were used, each spaced 2 cm apart, starting at 6 cm from the center of the fuel port, extending through the fuel port, and ending 20 cm from the center of the fuel port, as shown in Figure 16. Temperatures were simultaneously measured at elevations above the burner of 25 cm, 50 cm, 75 cm, and 100 cm, as shown in Figure 17. Each measurement position was held for 60 seconds and data was recorded at 10,000 Hz.
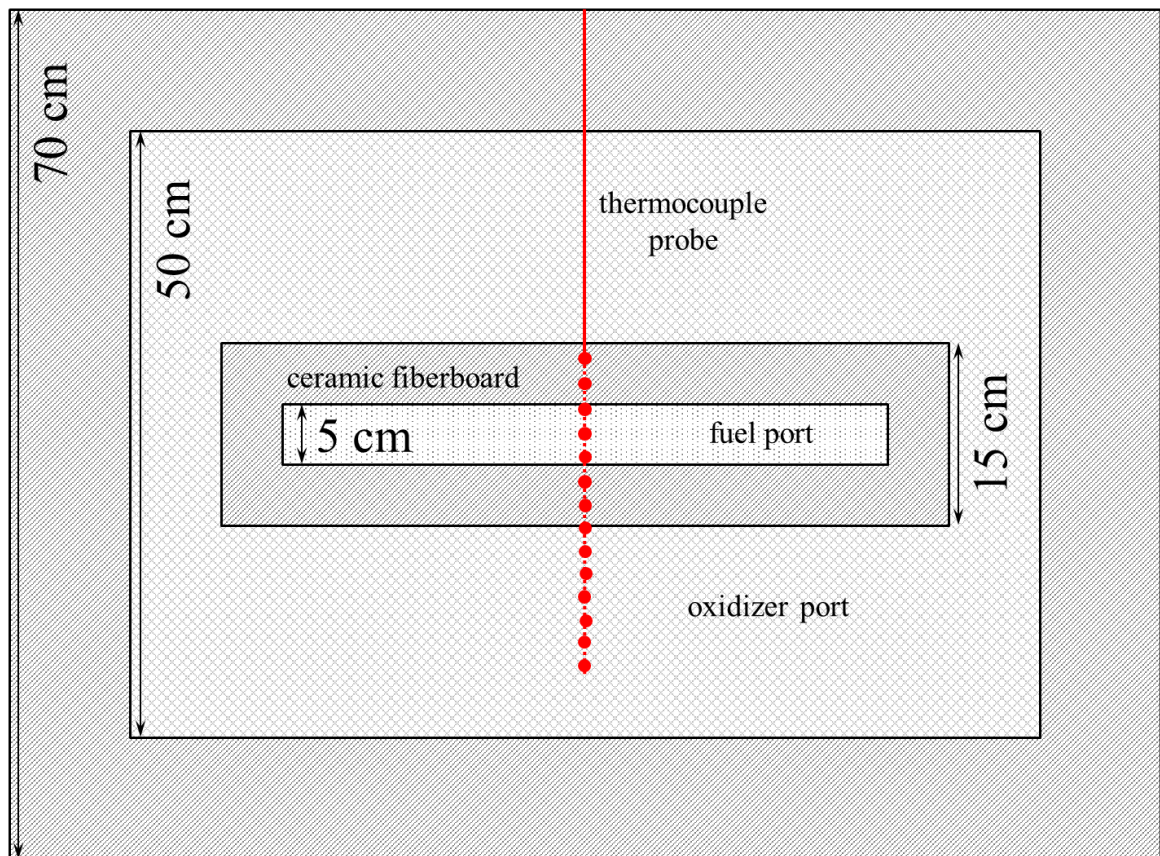
Figure 16 Thermocouple measurement points for cross-flame profile

Figure 17 Representative image of thermocouple positions above the burner surface (not to scale)

For the vertical centerline profile, only one thermocouple was used. The thermocouple was mounted 1 m above the surface of the center of the fuel port and lowered incrementally, to approximately 2 cm above the fuel port. Each measurement position was held for 60 seconds and data was recorded at 10,000 Hz.

Chapter 3: Results

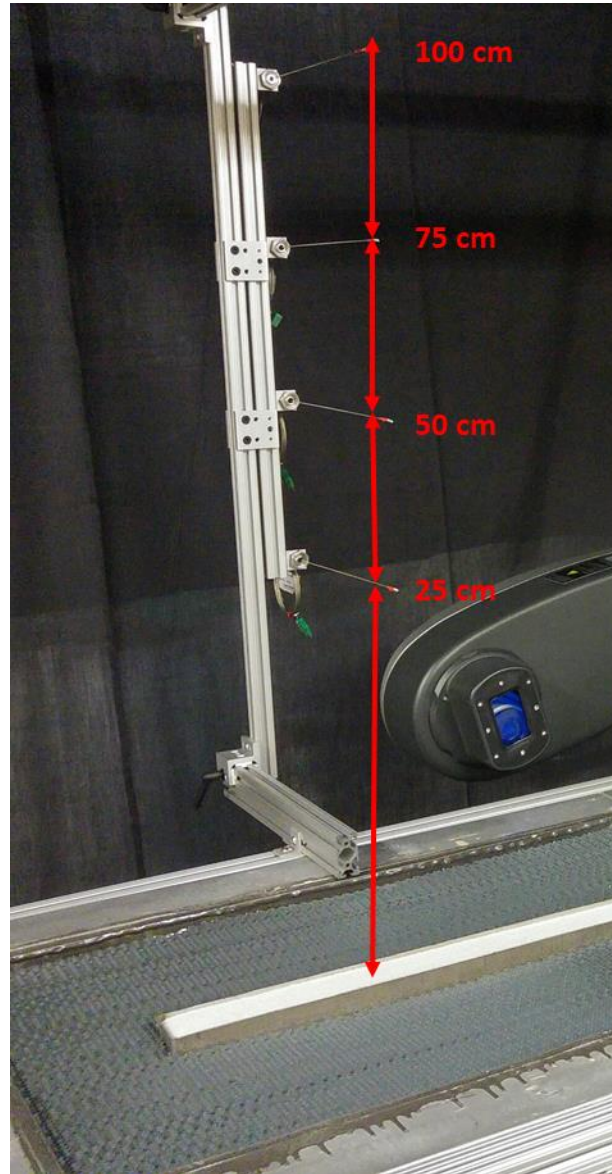## 3.1 Water Mist Suppression

Adjustments were made to the existing turbulent line burner facility to add to

and refine a water mist suppression system that provides controlled flame quenching

by introducing a fine water mist into the oxidizer stream. Suppression via water mist

occurs primarily as gas phase cooling, where evaporation of mist near the flame leads

to direct flame cooling due to the high latent enthalpy of vaporization of water

(approximately 2260 J/g). The evaporation of mist upstream from the flame also

contributes to suppression by increasing the water vapor mole fraction in the oxidizer,

which lowers the oxygen mole fraction in the oxidizer, yielding an oxidizer-dilution

effect similar to the nitrogen suppression experiments previously conducted [25],

where the additional water vapor in the combustion region dissipates heat from the

reaction and lowers the flame temperature.

Representative images depicting flame quenching behavior due to water mist

suppression are presented in Figure 18 at selected water mist mass loading conditions.

Images were recorded using a Canon EOS 40D digital camera with fixed exposure

settings, permitting direct comparison of the changes in flame luminosity observed at

each condition. Here, yellow flame regions are marked by the incandescence of soot

particles within the flame, where variations in luminous intensity indicate changes in

flame temperature and/or the local soot concentration. As shown in Figure 18, as the

mass loading of the water mist increases, there is a significant reduction in the

observable flame luminosity, attributable to diminishing soot incandescence

(representative of flame weakening), but also to the increasing attenuation of the visible flame emissions via Mie scattering within the mist.

For water mist concentrations less than 0.02, there are minimal observable suppression effects of the mist other than to shroud the flame, particularly in the base region where the mist is most dense (see image (b) in Figure 18). As shown with this condition, the base-injected mist follows natural convection around the flame, drawn upward with buoyant entrainment and covering the full flame length. For water mist concentrations of approximately 0.06, reduction in flame luminosity is more apparent, noted in the occasional wisps of flame that escape the mist layer, though large portions of the flame are thoroughly hidden from view due to scattering effects (see image (c) in Figure 18). At water mist concentrations of approximately 0.08, a significant reduction in soot incandescence is apparent throughout the flame, however, periodic flashes of brightness occur where the flame encounters regions of locally low mist density, indicating that sufficient soot is present in the flame to incandesce, but lower flame temperatures caused by mist cooling effects lead to reduced luminous intensity (see image (d) in Figure 18). For water mist concentrations greater than 0.09, the flame is observable only as a faint reddish glow behind the cloud of mist (see images (e) and (f) in Figure 18).
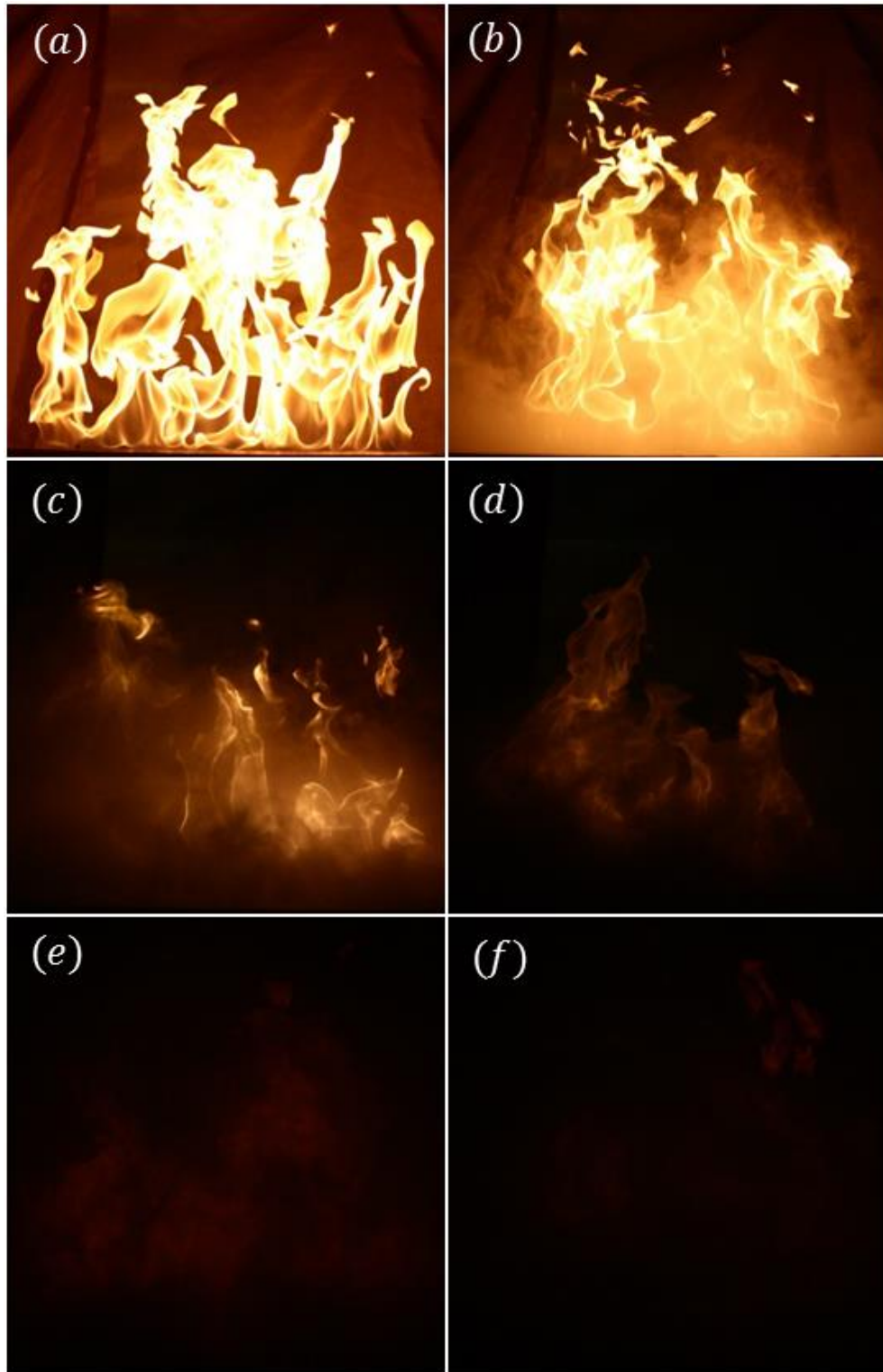
Figure 18 Front-view methane flame images ($\dot{Q}$ = 50 kW) at selected mist mass loadings; exposure: 1/1600 s, f/2.8, ISO-1600; (a) Y_{wm}^{ox} = 0.000, (b) Y_{wm}^{ox} = 0.023, (c) Y_{wm}^{ox} = 0.058, (d) Y_{wm}^{ox} = 0.077, (e) Y_{wm}^{ox} = 0.090, (f) Y_{wm}^{ox} = 0.093

Figure 19 provides images of significant points in the evolution of suppression to the point of extinction during one test:

- A 50 kW flame is stabilized at the burner (see image (a) in Figure 19).

- Water mist is introduced to the flame and an immediate reduction in luminosity is noted at the base of the flame (see image (b) in Figure 19).

- Imaging visibility is significantly reduced and observations indicate that the flame experiences drastic changes in size and structure within the mist cloud coupled with periods of flame-base destabilization and localized detachment from the fuel port (see images (c) through (e) in Figure 19).

- Once destabilized from the base, the flame is observed to lift and if conditions allow, reignite and reattach to the fuel port multiple times (see image (f) in Figure 19). Once a condition capable of extinguishing the flame is reached, observations suggest that several successive near-extinction events may occur before global extinguishment is achieved.

- Global flame extinction, occurring at Y_{wm}^{ox} equal to 0.093 ± 0.008, is observed after a lifted flame is reduced to a localized pocket of reaction (see image (g) in Figure 19) that is subsequently quenched without reigniting nearby unburned fuel (see image (h) in Figure 19).
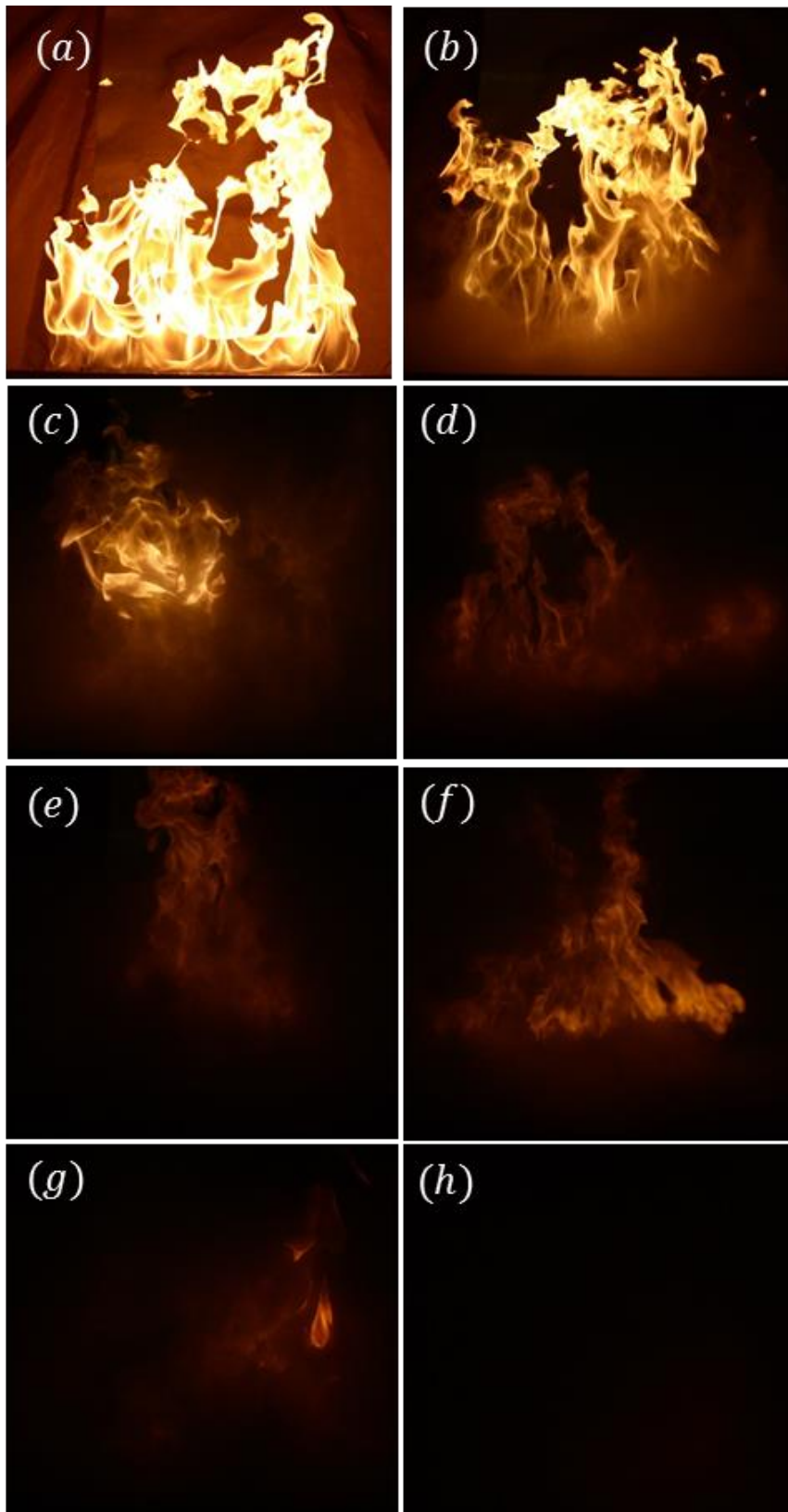
Figure 19 Interaction of flame with water mist; $Y_{wm}^{ox} = 0.093$

The reduction in flame luminosity shown in Figure 18 and Figure 19 is similar to previously reported observations for methane flames suppressed by dilution of the oxidizer with gaseous nitrogen [23]. Unlike suppression by nitrogen however, no significant portions of the mist-suppressed flames transition in color from yellow to blue, where blue flame regions indicate an absence of soot. This disparity suggests that soot production persists in spite of the suppression effects of the mist. The cooling potential of water mist is significantly greater than that for nitrogen due to the larger sensible heat capacity of water vapor and the latent contribution of droplet evaporation. As a result of this difference, a greater amount of nitrogen and, therefore, a lower oxygen concentration is required to achieve comparable flame cooling than that of water mist. The observed differences in soot-suppression behaviors between nitrogen and water mist are best attributed to the lower oxygen concentrations that occur at the nitrogen extinction limit, where soot production kinetics are highly sensitive to the local oxygen concentration [27] [28] [29].

Of further interest is the significant difference in the appearance of the water mist with the flame and without the flame. Without the flame, the water mist fills the containment system above the oxidizer port and rises all the way to the exhaust hood, as shown in Figure 7. With the flame, the water mist is observed to concentrate at the base of the flame, with some water mist escaping to rise higher in the flame zone. All of the water mist was consumed by the flame; none escaped into the exhaust system. As noted in other studies [22], the depletion of water mist in the presence of the flame is an indication of interaction between the water mist and the flame, resulting in the evaporation and consumption of water mist by the flame.

49

3.2 Calorimetry

The primary objective of the present work was to achieve global extinction of a 50 kW flame using only water mist as the suppressant in the existing turbulent line burner facility. While the visual observations detailed in Section 3.1 demonstrate extinction was achieved, extinction can also be measured using the existing calorimetry capabilities of the turbulent line burner facility. No adjustments were made to the instrumentation originally developed by White and measurements of total heat release rate ($\dot{Q}$) are derived via the calorimetry framework presented in Ref. [18], as summarized below. In applying this framework, the classical oxygen consumption (OC) and carbon dioxide generation (CDG) based formulations are utilized (neglecting soot production), given respectively as

$$\dot{Q}_{OC} = -\Delta h_{O_2}\dot{\omega}_{O_2} + (h_{O_2} - h_{O_2,CO})\left(\dot{\omega}_{CO}\frac{M_{O_2}}{2M_{CO}}\right) \tag{7}$$

and

$$\dot{Q}_{CDG} = \Delta h_{CO_2}\dot{\omega}_{CO_2} + (h_{CO_2} - h_{CO_2,CO})\left(\dot{\omega}_{CO}\frac{M_{CO_2}}{2M_{CO}}\right) \tag{8}$$

where Δh_{O_2} and Δh_{CO_2} are the mass-specific enthalpy differentials for oxygen and carbon dioxide, respectively, provided as referenced [24]. The terms for the mass reaction rate of the species ($\dot{\omega}_{O_2}$, $\dot{\omega}_{CO_2}$, and $\dot{\omega}_{CO}$) are evaluated from measurements of the exhaust flow rate and composition, coupled with a mass conservation analysis also described in [24].

From the calorimetry-derived $\dot{Q}$, the combustion efficiency (η_{comb}) is defined as

$$\eta_{comb} = \frac{\dot{Q}}{\dot{m}_{fuel}\Delta h_{comb}} \qquad (9)$$

which provides a dimensionless quantification of normalized flame strength and is an ideal metric for the assessment of suppression performance. For the presently reported combustion efficiency, the heat release rate in Equation (9) is evaluated as the average of $\dot{Q}_{OC}$ and $\dot{Q}_{CDG}$ determined using Equations (7) and (8).

An estimate of the convective fraction of the combustion heat release rate (χ_{conv}) is defined as

$$\chi_{conv} = \frac{\dot{m}_e c_{p,e}(T_e - T_\infty) + \dot{m}_{wm}^{vap}\Delta h_{H_2O}^{vap}}{\dot{m}_{fuel}\Delta h_{comb}} \qquad (10)$$

where the left numerator term estimates the heating required to achieve a measured temperature rise in the exhaust flow, while the right numerator term provides a correction to account for the latent heat removal of droplet evaporation. This expression assumes that all of the injected mist evaporates ($\dot{m}_{wm}^{vap} = \dot{m}_{wm}^{ox}$) and that no condensation occurs in the exhaust ductwork, as observed during the actual experiments.

Assuming that the remaining fraction of the combustion heat release rate is predominantly due to radiation losses, an estimate of the radiative loss fraction (χ_{rad}) is then determined via

$$\chi_{rad} = \eta_{comb} - \chi_{conv} \qquad (11)$$

where other heat losses, such as conduction losses to the walls of the exhaust ductwork or to the burner surface are neglected.

As defined in Equation (11), the radiative loss fraction is complicated by the effects of radiation attenuation in the mist and water vapor that envelop the flame.

51

Specifically, any radiative flame emissions that are absorbed by excess water vapor or mist around the flame are included in the convective fraction of the combustion heat release rate, as defined in Equation (10), and are, therefore, not accounted for in the radiative loss fraction. As a result, the present radiative loss fraction should only be interpreted as representing the fraction of radiative flame emissions that escape the mist.

Presently measured data for the combustion efficiency, convective fraction, and radiative loss fraction are plotted versus water mist mass fraction (Y_{wm}^{ox}) in Figure 20. As shown, the combustion efficiency is approximately equal to 1 for the full range of tested water mist mass loadings, with measured $\eta_{comb} = 0.96$ at $Y_{wm}^{ox} = 0.092$, immediately before global flame extinguishment occurs at $Y_{wm}^{ext} = 0.093$. This result reveals that despite the previously described suppression effects that are observed with increasing water mist mass loadings (consisting of reductions in flame luminosity and diminishing soot incandescence), complete combustion persists until the extinction limit is reached. Although the appearance of the flame is substantially different, this combustion behavior is in close agreement with recent measurements from the same configuration, but for flame suppression via dilution of the oxidizer with gaseous nitrogen [24].

The present results additionally agree with data reported for water mist suppression of a laminar forced boundary layer flame over a flat plate of PMMA, for which surface-regression based measurements of the local burning rate indicated that extinction occurred within a narrow suppression window outside of which variations in the concentration of the water mist had a negligible impact on burning rate [19].
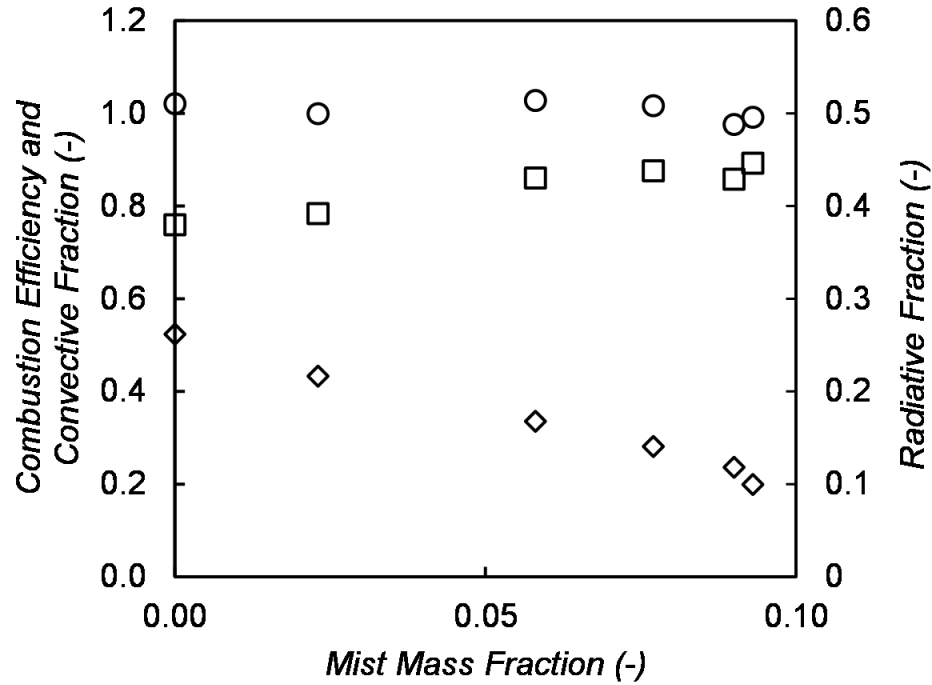
Figure 20 Calorimetry-derived combustion efficiency (noted as circles), convective fraction (noted as squares), and radiative fraction (noted as diamonds) plotted versus water mist mass fraction for a 50 kW methane diffusion flame

Also shown in Figure 20, the convective fraction of the combustion heat release rate increases quasi-linearly with rising concentrations of water mist, from approximately 0.76 at $Y_{wm}^{ox} = 0.0$ to approximately 0.87 at $Y_{wm}^{ox} = 0.09$. Correspondingly, the radiative loss fraction steadily decreases from approximately 0.26 at $Y_{wm}^{ox} = 0.0$ to approximately 0.12 at $Y_{wm}^{ox} = 0.09$. These trends are due primarily to the offsetting influences of T_e and $\dot{m}_{wm}^{vap}$ in Equation (9), where $\dot{m}_{wm}^{vap}$ intuitively increases directly with Y_{wm}^{ox}, while the measured T_e decreases only slightly from about 335 K at $Y_{wm}^{ox} = 0.0$ to about 325 K at $Y_{wm}^{ox} = 0.09$. Effectively, the slight decline in T_e does not fully account for the latent cooling effects of the additional evaporating droplets, indicating that the flame-mist interactions cause an increasing

fraction of the combustion heat to be convected into the exhaust flow. This observation is the result of two primary factors: first, the envelope of mist surrounding the flame captures part of the radiative flame emissions and then releases that heat back into the exhaust upon evaporation; and second, the radiative flame emissions are diminished as a result of declining flame temperatures, which combined with a constant η_{comb} indicates that a greater portion of the heat release must be retained by the flow.

In addition to combustion efficiency, net combustion yields are also possible from the experimental facility, as shown in Figure 21, the net combustion yield of CO_2 and Figure 22, the net combustion yield of CO. Each plot also includes the stoichiometric yield for each species, shown as a solid red line, defined as

$$y_{k,st} = v_{k,st} \left(\frac{M_k}{M_f} \right) \tag{12}$$

where M_k is the molar mass of the species k, M_f is the molar mass of the fuel, and $v_{k,st}$ is the molar reaction coefficient for species k in the balanced equation for the stoichiometric combustion of methane in air:

$$CH_4 + 2(O_2 + 3.76N_2) \longrightarrow CO_2 + 2H_2O + 0.5O_2 + 7.52N_2 \tag{13}$$
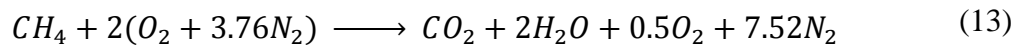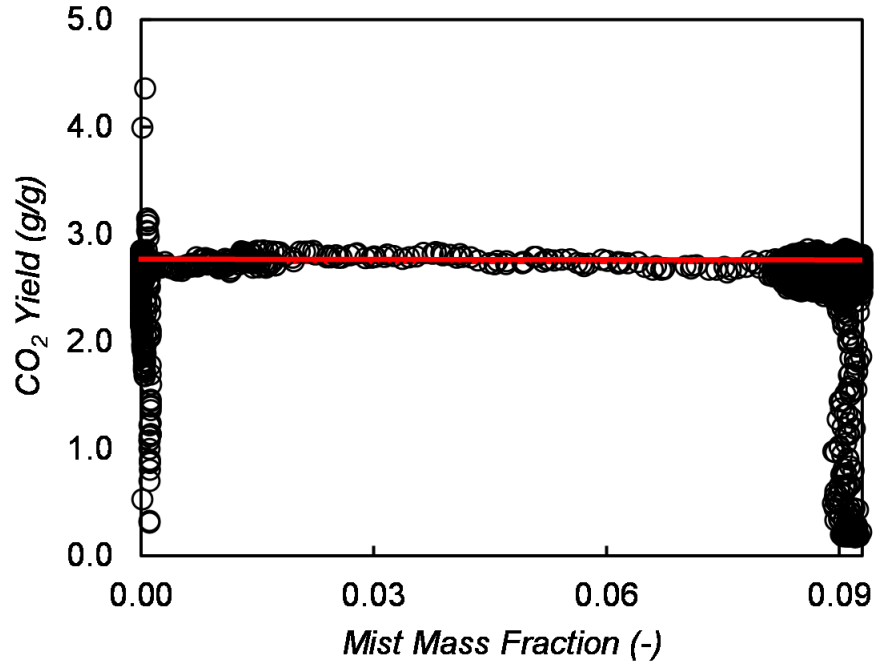
Figure 21 Carbon dioxide yield as a function of the mist mass fraction; stoichiometric yield shown as a solid red line
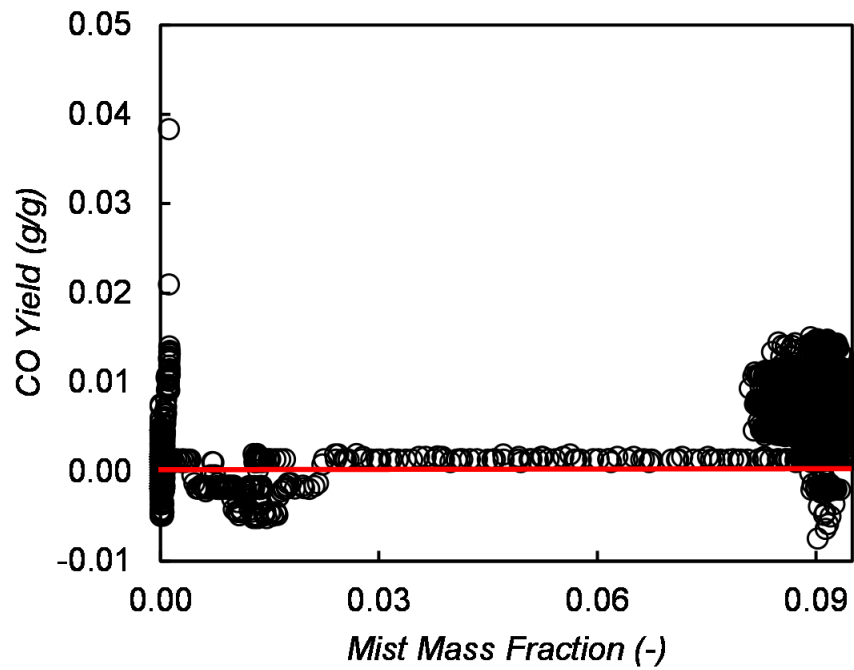

Figure 22 Carbon monoxide yield as a function of the mist mass fraction; stoichiometric yield shown as a solid red line

As shown in Figure 21 and Figure 22, the net combustion yield of carbon dioxide is approximately equal to the stoichiometric yield of 2.75 and the net combustion yield of carbon monoxide is approximately equal to the stoichiometric yield of 0. A small, nearly negligible increase in the carbon monoxide yield is noted at the moment of extinction. For carbon dioxide, as noted in the combustion efficiency data, there is no contribution of partial or incomplete combustion observed. At the moment of extinction, the fuel stops burning, and the production of carbon dioxide drops off.

The present work is the first to report this type of extinction behavior for water mist suppression of a large scale buoyant, turbulent diffusion flame and demonstrates that the calorimetry measurement methodology is capable of delivering reliable data for fires suppressed with water.

3.3 Temperatures

Temperatures were measured along the vertical centerline of a 50 kW flame and across the cross-flame profile of the flame. As shown in Figure 23, temperatures rose as the probe reached the edge of the burner, then peaked just over 1100 K at the center of the burner and at an elevation of 25 cm above the surface of the burner. The temperatures measured by the probe at 25 cm (closest to the burner surface) dropped sharply as the probe moved through the flame region and back out over the oxidizer port. Temperatures above the direct and constant reach of the flame at an elevation of 100 cm above the burner remained mostly steady at 500 K throughout the profile.

As shown in Figure 24, average temperatures along the vertical centerline of the flame peaked at approximately 1180 K, 13 cm above the surface of the burner. At elevations lower than 13 cm, temperatures were slightly lower, indicating the region where cooler fuel still remains. Once reaching the peak at 13 cm, temperatures then gradually decreased in a linear fashion before leveling off at 500 K, 100 cm above the surface of the burner. These measurements are in agreement with the work by McCaffery, who evaluated the temperatures in turbulent methane diffusion flames and found that slightly above the base of the fire in the continuous flame region, temperatures are approximately 1170 K [30].

A sample time trace plot measured at 13 cm is provided in Figure 25, where the peak temperature recorded is approximately 1910 K and the standard deviation across the full 60 second signal is 382 K. The peak recorded temperature is lower than the adiabatic flame temperature for methane of 2222 K [31], but within the expected range due to radiation losses. The large standard deviation in the

measurements is due to the turbulence in the flame and flows and confirms the

responsiveness of the thermocouples to fast changes in the combustion region.
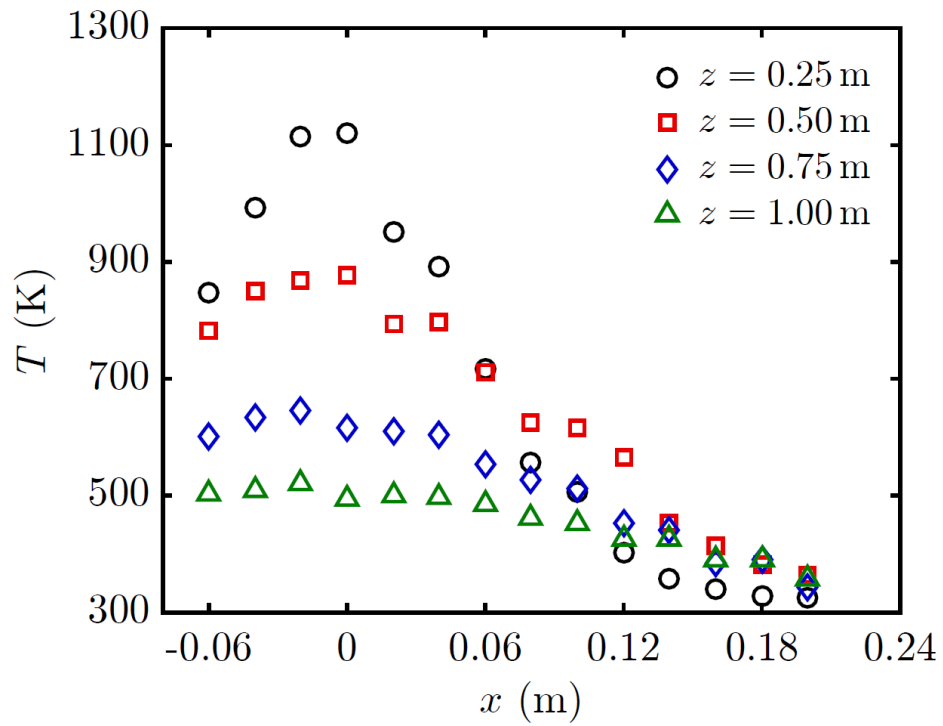

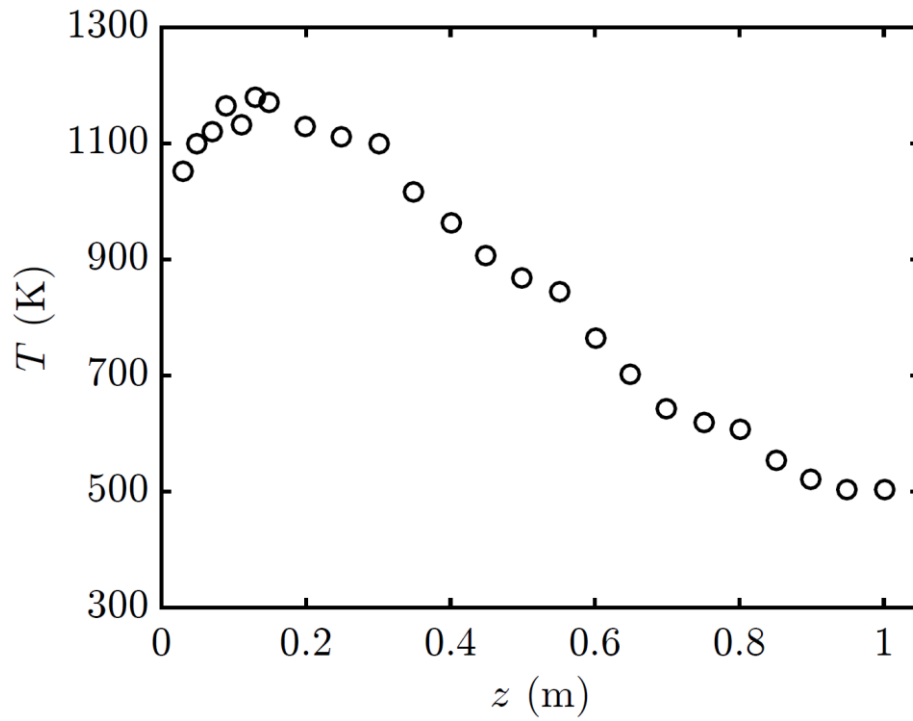*Figure 23 Cross-flame temperature profiles for 50 kW flame at varying elevations (z)*

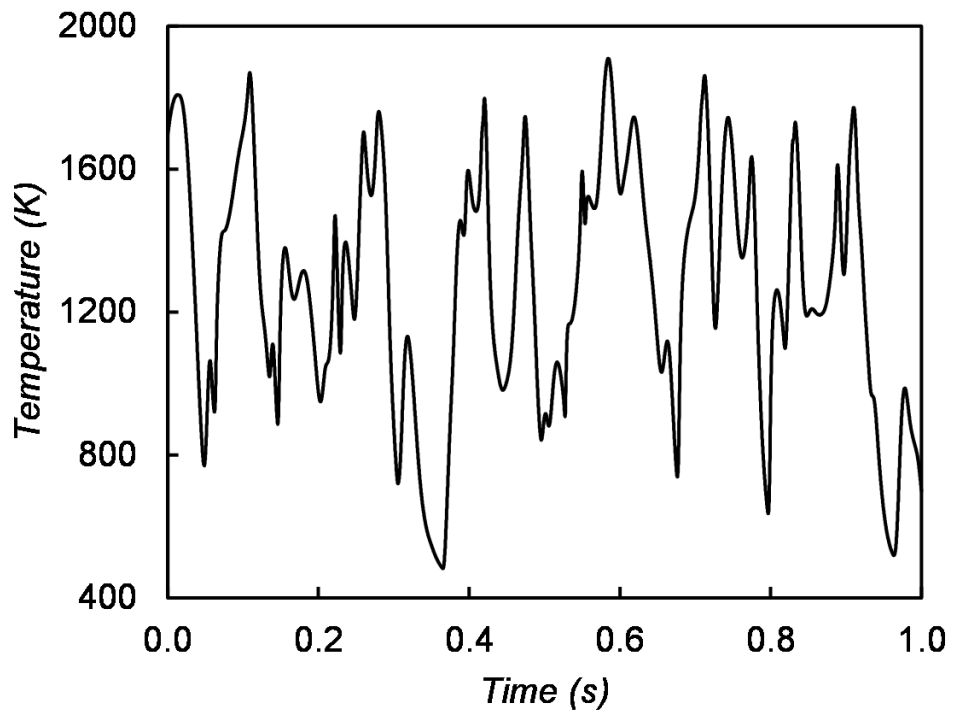*Figure 24 Vertical centerline temperature profiles for 50 kW flame*

Figure 25 Sample time trace at 13 cm above the surface of the burner

Chapter 4: Conclusion and Future Work

The primary objective of the this work was to provide a detailed experimental study of water mist fire suppression phenomena in a buoyant, turbulent diffusion flame representing the key characteristics of a realistic fire. The experimental configuration features an existing laboratory scale facility that has been proven to provide well-characterized inlet and boundary conditions suitable for application to CFD fire simulations for nitrogen-based suppression experiments, wherein the facility was modified to allow for the use of water mist, while still taking advantage of the existing classical species-based calorimetry techniques the facility provides to quantify water mist suppression performance. In addition, a secondary objective of this work was to collect turbulent flame temperature data, such that future work can accurately determine the interaction of the water mist with the flame. The primary goal of this work is to provide a detailed dataset suitable to support the development and validation of predictive fire suppression models by developing water mist suppression capabilities in the existing turbulent line burner apparatus.

Multiple adjustments in the control system were made to the existing turbulent line burner facility to allow for increased water mist generation efficiency, including streamlining of the oxidizer delivery system to reduce friction losses and increase oxidizer flow, water level improvements to increase mist generation efficiency, the addition of a larger honeycomb at the top of the oxidizer to allow water mist droplets to pass through while still serving as a flow straightener, the addition of a mist containment system to homogenize the water mist in the flame region, and increased exhaust flow inside the containment system to further improve the water mist

distribution in the flame region and to reduce secondary flows. Following these improvements, the capabilities of the water mist generation system were characterized both using a classical mass balance approach and using more modern technology based techniques.

Species-based calorimetry was used to evaluate the global heat release rate and combustion efficiency of a 50 kW methane flame suppressed using the water mist system developed. The analysis of global suppression performance indicate the persistence of stoichiometric combustion, with an abrupt transition to complete extinguishment occurring only at the extinction limit, which was determined to be a water mist mass loading of approximately 0.093. The present work is the first to report this type of extinction behavior for water mist suppression of a large scale buoyant, turbulent diffusion flame and demonstrates that the calorimetry measurement methodology is capable of delivering reliable data for fires suppressed with water.

Previous work has suggested that for very fine droplets comparable to those in the present study (smaller than 10 µm), all drops should evaporate well outside the flame sheet and that the flame experiences only a fraction of the latent cooling potential of the droplets. When applied to the present results however, this rationale is not fully supported. Considering the present extinction results and assuming complete evaporation of all injected mist, the measured extinction limit of $Y_{wm}^{ext} = 0.093$ is comparable to previously reported extinction limits for droplets of a similar size (different fuel) and lower than previously reported extinction limits for larger droplets used to suppress laminar methane flames. It is suspected that turbulence may

play a role in the extinction behavior, where turbulent mixing should encourage flame interaction with the droplet cooled oxidizer, even if such cooling occurs outside the flame sheet. Additional turbulent mist extinction testing in buoyancy-driven configurations is necessary to further support this hypothesis, where previous work in a counter-flow configuration has already shown that mist suppression performance is sensitive to the strain rate at the flame sheet. Previous works have also shown that the turbulence induced by high-pressure mist nozzles can also enhance combustion and hinder suppression performance.

In conjunction with this work, detailed local measurements of flame temperature were performed and provide a useful data set for the evaluation of flame suppression response and for the validation of CFD fire models.

The long-term goal of this work is the continued successful realization of performance-based design methods for fire suppression systems. In order to achieve this goal, further analytical design tools are required based on a fundamental understanding of suppression phenomena. With the added capability of water mist suppression in the turbulent line burner facility and the addition of the thermocouple apparatus, additional diagnostics can be added to investigate the penetration of droplets into the flame. Further analysis of the thermocouple temperature data is also possible to determine whether or not there is mixing between the flame and the cooler, entrained air just outside the flame sheet. Further work may also include further calorimetry analysis and the use of an alternate fuel, such as propane.

Bibliography

[1] A. M. Lentati, H. K. Chelliah, Dynamics of water droplets in a counterflow field and their effect on flame extinction, Combustion and Flame 115 (1) (1998) pp. 158-179.

[2] A. Yoshida, T. Uendo, R. Takasaki, H. Naito, Y. Saso, Water droplets behavior in extinguishing methane-air counterflow diffusion flames, in: Fire Safety Science-Proceedings of the Tenth International Symposium, IAFSS, 2011, pp. 569-582.

[3] P. E. Santangelo, P. Tartarini, Fire control and suppression by water-mist systems, Open Thermodynamics Journal 4 (4) (2010) pp. 167-184.

[4] NFPA 750, *Standard on water mist fire protection systems*, NFPA, www.nfpa.org (2015).

[5] K. Prasad, C. Li, K. Kailasanath, Simulation of water mist suppression of small scale methanol liquid pool fires, Fire Safety Journal 33 (3) (1999) pp. 185-212.

[6] I. Sakurai, J. Suzuki, Y. Kotani, H. Naito, A. Yoshida, Extinguishment of propane/air co-flowing diffusion flames by fine water droplets, Proceedings of the Combustion Institute 34 (2) (2013) pp. 2727-2734.

[7] A. M. Lentati, H. K. Chelliah, Physical, thermal, and chemical effects of fine-water droplets in extinguishing counterflow diffusion flames, Proceedings of the Combustion Institute 27 (2) (1998) pp. 2839-2846.

[8] R. Ananth, R. C. Mowrey, Ultra-fine water mist extinction dynamics of a co-flow diffusion flame, Combustion Science and Technology 180 (9) (2008) pp. 1659-1692.

[9] A. K. Lazzarini, R. H. Krauss, H. K. Chelliah, G. T. Linteris, Extinction conditions of non-premixed flames with fine droplets of water and water/NaOH solutions, Proceedings of the Combustion Institute 28 (2) (2000) pp. 2939-2945.

[10] T. M. Jayaweera, H.-Z. Yu, Scaling of fire cooling by water mist under low drop Reynolds number conditions, Fire Safety Journal 43 (1) (2008) pp. 63-70.

[11] B. T. Fisher, A. R. Awtry, R. S. Sheinson, J. W. Fleming, Flow behavior impact on the suppression effectiveness of sub-10-µm water drops in propane/air co-flow non-premixed flames, Proceedings of the Combustion Institute 31 (2) (2007) pp. 2731-2739.

[12]   A. Jenft, A. Collin, P. Boulet, G. Pianet, A. Breton, A. Muller, Experimental and numerical study of pool fire suppression using water mist, Fire Safety Journal 67 (2014) pp. 1-12.

[13]   C. C. Ndubizu, R. Ananth, P. A. Tatem, Expermental study of fire suppression with water mist: 1. Small gaseous diffusion flame, Naval Research Laboratory Report NFL/MR/6180-98-8157, April 15, 1998.

[14]   E. Blanchard, S. Desanghere, P. Boulet, Quantification of energy balance during fire suppression by water mist in a mid-scale test tunnel, in: Fire Safety Science-Proceedings of the Tenth International Symposium, IAFSS, 2011, pp. 119-132.

[15]   H. Shilling, B. Z. Dlugogorski, E. M. Kennedy, Extinction of diffusion flames by ultrafine water mist doped with metal chlorides, in: Proceedings of the Sixth Australasian Heat and Mass Transfer Conference, AFTES, 1996, pp. 275–282.

[16]   K. Prasad, C. Li, K. Kailasanath, C. C. Ndubizu, R. Ananth, P. A. Tatem, Numerical modeling of water mist suppression of methane-air diffusion flames, Combustion Science and Technology 132 (1998) pp. 325-364.

[17]   E. J. P. Zegers, B. A. Williams, R. S. Sheinson, J. W. Fleming, Dynamics and suppression effectiveness of monodisperse water droplets in non-premixed counterflow flames, Proceedings of the Combustion Institute 28 (2) (2000) pp. 2931-2937.

[18]   G. O. Thomas, The quenching of laminar methane-air flames by water mists, Combustion and Flame 130 (1) (2002) pp. 147-160.

[19]   C. C. Ndubizu, R. Ananth, F. W. Williams, Water mist suppression of PMMA boundary layer combustion – A comparison of NanoMist and spray nozzle performance, Technical Report NRL/MR/6180–04-8824, NRL, 2004.

[20]   R. Ananth, C. C. Ndubizu, F. W. Williams, A numerical model for water mist suppression of a solid plate in boundary layer flow, in: Halon Options Technical Working Conference, NMERI (2004) pp. 1-10.

[21]   A. Yoshida, K. Kashiwa, S. Hashizume, H. Naito, Inhibition of counterflow methane/air diffusion flame by water mist with varying mist diameter, Fire Safety Journal 71 (2015) pp. 217-225.

[22]   K. C. Adiga, R. F. Hatcher, R. S. Sheinson, F. W. Williams, S. Ayers, A computational and experimental study of ultra fine water mist as a total flooding agent, Fire Safety Journal 42 (2) (2007) pp. 150-160.

[23] J. P. White, E. D. Link, A. C. Trouve, P. B. Sunderland, A. W. Marshall, J. A. Sheffel, M. L. Corn, M. B. Colket, M. Chaos, H. Z. Yu, Radiative emissions measurements from a buoyant, turbulent line flame under oxidizer-dilution quenching conditions, Fire Safety Journal 76 (2015) pp. 74-84.

[24] J. P. White, E. D. Link, A. C. Trouve, P. B. Sunderland, A. W. Marshall, A general calorimetry framework for measurement of combustion efficiency in a suppressed turbulent line fire, Fire Safety Journal (2016), submitted for publication.

[25] J. P. White, Measurement and simulation of suppression effects in a buoyant turbulent line fire, Dissertation, University of Maryland, 2016.

[26] W. Wagner, A. Pruß, The IAPWS formulation 1995 for the thermodynamic properties of ordinary water substance for general and scientific use, Journal of Physical and Chemical Reference Data 31 (2) (2002) pp. 387-535.

[27] K. C. Smyth, J. H. Miller, R. C. Dorfman, W. G. Mallard, R. J. Santoro, Soot inception in a methane/air diffusion flame as characterized by detailed species profiles, Combustion and Flame 62 (2) (1985) pp. 157-181.

[28] J. Du, R. L. Axelbaum, The effect of flame structure on soot-particle inception in diffusion flames, Combustion and Flame 100 (3) (1995) pp. 367-375.

[29] R. A. Dobbins, Soot inception temperature and the carbonization rate of precursor particles, Combustion and Flame 130 (3) (2002) pp. 204-214.

[30] B. J. McCaffrey, Purely buoyant diffusion flames: some experimental results (NBSIR 79-1910), U.S. National Bureau of Standards, Gaithersburg, MD (1979).

[31] V. Babrauskas, Temperatures in flames and fires, Fire Science and Technology Inc., http://www.doctorfire.com/flametmp.html (2016).